

## RESEARCH ARTICLE

# SLC25A46 promotes mitochondrial fission and mediates resistance to lipotoxic stress in INS-1E insulin-secreting cells

Jaime Santo-Domingo<sup>1,2,\*</sup>, Steve Lassueur<sup>1</sup>, Antonio Núñez Galindo<sup>4</sup>, Pilar Alvarez-Illera<sup>2</sup>, Silvia Romero-Sanz<sup>2</sup>, Elena Caldero-Escudero<sup>2</sup>, Sergio de la Fuente<sup>3</sup>, Loïc Dayon<sup>4,5</sup> and Andreas Wiederkehr<sup>1,5</sup>

**ABSTRACT**

Glucose sensing in pancreatic  $\beta$ -cells depends on oxidative phosphorylation and mitochondria-derived signals that promote insulin secretion. Using mass spectrometry-based phosphoproteomics to search for downstream effectors of glucose-dependent signal transduction in INS-1E insulinoma cells, we identified the outer mitochondrial membrane protein SLC25A46. Under resting glucose concentrations, SLC25A46 was phosphorylated on a pair of threonine residues (T44/T45) and was dephosphorylated in response to glucose-induced  $\text{Ca}^{2+}$  signals. Overexpression of SLC25A46 in INS-1E cells caused complete mitochondrial fragmentation, resulting in a mild mitochondrial defect associated with lowered glucose-induced insulin secretion. In contrast, inactivation of the *Slc25a46* gene resulted in dramatic mitochondrial hyperfusion, without affecting respiratory activity or insulin secretion. Consequently, SLC25A46 is not essential for metabolism–secretion coupling under normal nutrient conditions. Importantly, insulin-secreting cells lacking SLC25A46 had an exacerbated sensitivity to lipotoxic conditions, undergoing massive apoptosis when exposed to palmitate. Therefore, in addition to its role in mitochondrial dynamics, SLC25A46 plays a role in preventing mitochondria-induced apoptosis in INS-E cells exposed to nutrient stress. By protecting mitochondria, SLC25A46 might help to maintain  $\beta$ -cell mass essential for blood glucose control.

**KEY WORDS:** Mitochondria,  $\beta$ -cell, Mitochondrial dynamics, Phosphorylation, Lipotoxicity, SLC25A46

**INTRODUCTION**

Stimulation of pancreatic  $\beta$ -cells by glucose promotes secretion of insulin, the hormone that lowers blood glucose following a meal.  $\beta$ -cells sense glucose via its uptake and metabolism (de Vos et al., 1995; Schuit et al., 1997). Mitochondria are playing an essential role in this process by oxidizing glucose-derived pyruvate. Acute stimulation of  $\beta$ -cells with glucose enhances mitochondrial  $\text{CO}_2$  production, oxygen consumption and mitochondrial ATP synthesis rates as part of the sensing mechanism leading to an adapted insulin

secretory response (Antinozzi et al., 2002; de Marchi et al., 2014; Hellman et al., 1974; Santo-Domingo et al., 2019; Wiederkehr and Wollheim, 2012). Mitochondrial metabolism also generates metabolic signals, most importantly ATP, which inhibits the plasma membrane  $\text{K}_{\text{ATP}}$  channel. Closure of the  $\text{K}_{\text{ATP}}$  channel depolarizes the  $\beta$ -cell, which leads to  $\text{Ca}^{2+}$  influx through voltage-gated  $\text{Ca}^{2+}$  channels and the stimulation of exocytosis (Rorsman and Ashcroft, 2018; Wiederkehr and Wollheim, 2012).


Pancreatic  $\beta$ -cells contain densely packed mitochondria composed of multiple juxtaposed filamentous networks (Molina et al., 2009; Park et al., 2008; Twig et al., 2008). These networks are in constant motion and their filaments undergo continuous remodeling (Griesche et al., 2019; Molina et al., 2009) through the fusion of mitochondria with each other and the fission into shorter mitochondrial units. Mitochondrial fission requires dynamin-related protein 1 (Drp1; also known as DNM1L), which binds to outer mitochondrial membrane receptors where it couples GTP hydrolysis to mitochondrial fission. Mitofusins (Mfn1 and Mfn2) and autosomal dominant optic atrophy 1 (OPA1) are the GTPases responsible for mitochondrial fusion (Liesa et al., 2009). Pronounced fragmentation or alternatively mitochondrial swelling in combination with mitochondrial aggregation can be observed following manipulation of proteins of the fission and fusion machineries in  $\beta$ -cells (Hennings et al., 2018; Molina et al., 2009; Park et al., 2008). The knockout of several fission fusion genes perturbs mitochondrial function and/or glucose-induced insulin secretion (Hennings et al., 2018; Park et al., 2008; Zhang et al., 2011).

Several of these core-shaping proteins also control the ultrastructural organization of mitochondria, for example at the level of cristae of the inner mitochondrial membrane (Frezza et al., 2006; Neupert, 2012) and, hence, directly or indirectly regulate energy metabolism (Liesa et al., 2009; Park et al., 2008; Pich et al., 2005). OPA1, for example, controls cristae junctions to maintain normal inner mitochondrial membrane compartmentalization (Frezza et al., 2006; Olichon et al., 2003). Consistent with this function, mitochondria in  $\beta$ -cells lacking OPA1 are short with highly disorganized cristae (Zhang et al., 2011). OPA1-knockout islets display reduced respiratory chain activity, a poor respiratory response to glucose and fail to secrete insulin *in vivo* resulting in severely impaired glucose tolerance (Zhang et al., 2011). However, aggregation of mitochondria alone is not sufficient to impair energy metabolism and insulin secretion in  $\beta$ -cells (Hennings et al., 2018; Park et al., 2008).

Proteins of the fission and fusion machineries also play an important role in the regulation of apoptosis (Lee et al., 2004; Liesa et al., 2009). One mechanism linking OPA1 or Drp1 to apoptosis is through the regulation of cristae morphology and the release of apoptogenic factors, including cytochrome *c*, in response to cellular stress (Frezza et al., 2006; Germain et al., 2005).  $\beta$ -cells are nutrient sensors but suffer when exposed chronically to elevated glucose or

<sup>1</sup>Department of Cell Biology, Nestlé Institute of Health Sciences, Nestlé Research, CH-1015 Lausanne, Switzerland. <sup>2</sup>Department of Biochemistry and Molecular Biology, Unidad de Excelencia Instituto de Biología y Genética Molecular (IBGM), Faculty of Medicine, 47003 Valladolid, Spain. <sup>3</sup>Center for Translational Medicine, Department of Medicine, Thomas Jefferson University, Philadelphia, PA 19107, USA. <sup>4</sup>Proteomics, Nestlé Institute of Food Safety & Analytical Sciences, Nestlé Research, CH-1015 Lausanne, Switzerland. <sup>5</sup>Ecole Polytechnique Fédérale de Lausanne, CH-1015 Lausanne, Switzerland.

\*Author for correspondence (jaime.santo-domingo@uva.es)

 L.D., 0000-0002-8499-270X; A.W., 0000-0003-2685-7558

Handling Editor: Jennifer Lippincott-Schwartz  
Received 29 March 2022; Accepted 1 March 2023

lipids (Eizirik et al., 1992; El-Assaad et al., 2003; Maedler et al., 2001; Molina et al., 2009; Shah et al., 2013). Exposure of  $\beta$ -cells to lipotoxic conditions causes fragmentation of mitochondria by suppressing their ability to undergo mitochondrial fusion, which occurs even before apoptosis is initiated (Molina et al., 2009). Chronic high glucose has only minor effects on mitochondrial morphology, although acute glucose stimulation causes transient fragmentation and re-localization of mitochondria in insulin-secreting cells (Griesche et al., 2019; Jhun et al., 2013; Molina et al., 2009). Preventing mitochondrial fragmentation (after knockdown of Fis1) protected insulin secreting cells from lipotoxicity-induced apoptosis (Molina et al., 2009) consistent with earlier findings showing that downregulation of Fis1 delays cytochrome *c* release and apoptosis (Lee et al., 2004).

Dominant optic atrophy and Charcot–Marie–Tooth type 2 are hereditary neurodegenerative disorders frequently caused by mutations in OPA1 or MFN2, respectively. More recently, loss-of-function mutants of SLC25A46 were found in families with members displaying both optic atrophy and axonal peripheral neuropathy (Abrams et al., 2015). SLC25A46 is an outer mitochondrial membrane protein important for the regulation of mitochondrial fission and the maintenance of mitochondrial cristae structure (Abrams et al., 2015; Janer et al., 2016). These findings establish links between altered mitochondrial dynamics, the control of cristae structure and hereditary neuropathies.

Here, we identify SLC25A46 as a mitochondrial phosphoprotein and important regulator of mitochondrial dynamics in insulin-secreting  $\beta$ -cells. SLC25A46 is phosphorylated on threonine T44 and T45. During acute glucose stimulation, SLC25A46 is dephosphorylated in a calcineurin-dependent manner. Phosphoregulation modulates the effect of SLC25A46 on mitochondrial dynamics. Disruption of SLC25A46 in INS-1E insulinoma cells causes pronounced hyperfilamentation of mitochondria, whereas mitochondrial respiration and glucose-induced insulin secretion are preserved. Importantly, lack of SLC25A46 function sensitizes the insulin-secreting cells to lipotoxicity.

## RESULTS

### Glucose-dependent SLC25A46 phosphorylation in INS-1E insulinoma cells

Through the analysis of the phosphoproteome in the INS-1E rat insulin-secreting cell line, we have previously described glucose-dependent protein phosphorylation and dephosphorylation events involved in biological processes ranging from insulin biosynthesis, vesicle trafficking to insulin granule exocytosis and cytoskeleton remodeling (Santo-Domingo et al., 2019) consistent with several related studies with insulinoma cells and primary  $\beta$ -cells. Our experimental setup was to follow glucose-dependent phosphorylation changes over three time-points (5, 30 and 60 min) in the presence of maximal stimulatory glucose (16.7 mM) and compare the phosphoproteome to the one of INS-1E cells maintained for the same duration under resting glucose conditions (2.5 mM). Following new analysis of the data (see Materials and Methods), we identified herein 37 additional mitochondrial peptides (sometimes containing multiple serine and/or threonine residues) with putative phosphorylation site(s) but where the exact localization of the modification(s) was still uncertain (Fig. 1A; Tables S1–S3). The strongest glucose-induced fold change was observed for a 22-amino-acid di-phosphorylated peptide within the mitochondrial membrane protein SLC25A46 (Fig. 1B). This study thus focuses on the glucose-dependent regulation of SLC25A46 and the role of this

protein in the control of mitochondrial function during stimulus secretion coupling in INS-1E cells.

SLC25A46 has six predicted transmembrane domains, which is similar to the number found in other members of the SLC25 family of mitochondrial carriers. The phosphopeptide identified here is localized on the N-terminal domain flanking the first transmembrane domain of SLC25A46 (Fig. 1B). The identified peptide contains six potential phosphorylation sites. Serine and threonine residues in this sequence are conserved between mammalian species. The pair of threonine residues (T44 and T45; hereafter T44/T45) on SLC25A46 is even conserved with more distant species including chicken, frog and zebrafish (Fig. 1B).

After stimulation of INS-1E cells with 16.7 mM glucose, phosphorylation of this phosphopeptide was reduced compared to the level seen in control cells maintained in basal (2.5 mM) glucose (Fig. 1C). In this respect, phosphorylation changes in this peptide behaved similarly to the autophosphorylation site S108 on the  $\beta$ -subunit of the energy sensor AMP-activated protein kinase (AMPK) (Fig. 1D).

Based on the proteomic data, the highest probability of phosphorylation localizations was assigned automatically by the Scaffold PTM software to S35 and T45, concomitantly, but still with a very limited confidence (i.e. 40%). Manual inspection of tandem mass spectra revealed in fact inconclusive for localization of the phosphorylation modifications on S35 or T37 one side and T44 or T45 on the other side. To validate T45 and the neighboring T44 as sites of glucose-dependent phosphorylation, we raised polyclonal antibodies against SLC25A46 peptides phosphorylated on T44 and T45 (see Materials and Methods). The antibodies recognized a protein of ~46 kDa (Fig. 1E) consistent with the predicted size of SLC25A46 (Fig. 1E,F) and a band of the same size was detected with a commercial antibody raised against SLC25A46 (Fig. 1G). The western blot signals were lost after  $\lambda$ -phosphatase treatment of INS-1E lysates (Fig. 1E) demonstrating our antibodies recognize the phosphorylated form of SLC25A46. Furthermore, our phospho-specific antibodies recognized a DDK-tagged SLC25A46 protein (SLC25A46-DDK) but failed to detect the phospho-null mutant (SLC25A46 A44/A45-DDK) when these transgenes were expressed in INS-1E cells. The commercial SLC25A46 antibody recognized both exogenously expressed wild-type and phosphorylation mutant proteins (Fig. 1G). Jointly, these findings show that our antibodies recognize the phosphorylated SLC25A46 epitope.

Western blotting using the phosphorylation-specific antibodies confirmed that glucose levels strongly affected the phosphorylation status of SLC25A46 on T44/T45 as already suggested by our mass spectrometry results. The phosphorylation status of T44/T45 of SLC25A46 increased with time (5–60 min) when INS-1E cells were transferred from culture medium (11 mM glucose) to a sub-stimulatory glucose concentration (2.5 mM). This increase was strongly attenuated in glucose-stimulated (16.7 mM) INS-1E cells (Fig. 1F). We conclude that the phosphorylation status of SLC25A46 on T44/T45 is regulated by glucose-induced signal transduction. SLC25A46 phosphorylation is maximal in resting INS-1E cells whereas stimulatory glucose promotes dephosphorylation of the protein.

### Glucose-driven SLC25A46 T44/T45 dephosphorylation is mediated by calcineurin

Searches using the NetPhos 3.1 software did not reveal any high-confidence kinase substrate consensus motif sequence around the T44/T45 phosphorylation site (data not shown). Given the close correlation between glucose-induced AMPK<sub>S108</sub> and

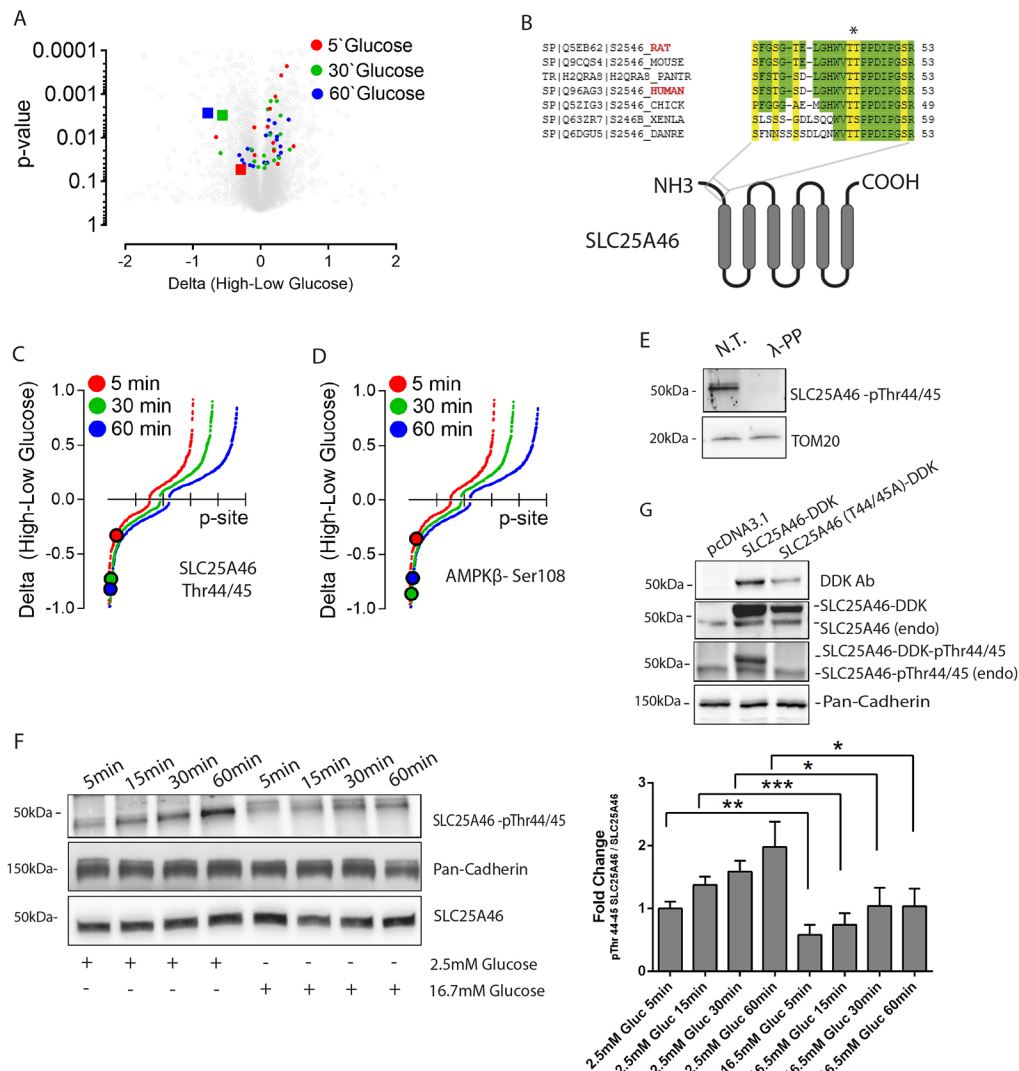


**Fig. 1. Identification of SLC25A46 as a glucose-regulated mitochondrial phosphoprotein in INS-1E cells.** (A) Phosphorylation changes of phosphopeptides after stimulation of INS-1E cells with 16.7 mM glucose for 5 min (red), 30 min (green) and 60 min (blue). The values shown were obtained after subtraction of the phospho-peptide abundance in low 2.5 mM glucose. The *P*-values assessing the differences before and after glucose stimulation were obtained from four independent experiments. Phosphorylations of the identified SLC25A46 peptide are shown as squares. Results are presented as volcano plots. (B) Alignment of the SLC25A46 peptide containing threonine residues T44 and T45 from different species. The position of this peptide at the N-terminus of the protein, close to the predicted first transmembrane domain is shown. (C,D) Peptides were ranked according to the difference (delta) in phosphorylation before and after glucose stimulation for the indicated times. (C) SLC25A46-T44/T45 and (D) AMPKβ-S108 phosphorylation levels are respectively displayed as larger circles (values represent the mean of five similar experiments). (E) Western blots demonstrating SLC25A46 T44/45 phosphorylation under non-stimulatory conditions with an antibody raised against double (pThr44/45) phosphorylated SLC25A46. INS-1E lysates were either non-treated (N.T.) or λ-phosphatase (λ-PP)-treated. (F) Western blot and bar graph showing the effect of glucose stimulation on SLC25A46 T44/45 phosphorylation followed with antibody raised against the double (pThr44/45) phosphorylated SLC25A46 (same antibody as for E). INS-1E cells were incubated with two glucose concentrations, respectively (2.5 and 16.7 mM), for increasing amounts of time as indicated. Bar graph shows mean±s.e.m. of six independent experiments (*n*=6). (G) Western blots demonstrating the specificity of the antibody recognizing the phosphorylated (pThr44/45) SLC25A46 protein in lysates from control cells, cells transfected with DDK-tagged version of wild type SLC25A46 and cells transfected with a DDK-tagged version encoding a double alanine mutant SLC25A46 A44/A45. Blots shown in F and G are representative of three repeats. \**P*<0.05; \*\**P*<0.01; \*\*\**P*<0.001 (two-tailed paired *t*-test).

SLC25A46<sub>T44/T45</sub> dephosphorylation kinetics (Fig. 1C,D), we tested whether energy stress is responsible for the observed elevated phosphorylation under sub-stimulatory glucose concentrations. We find that respiratory chain inhibitors and uncouplers known to activate AMPK decreased rather than increased the phosphorylation status of SLC25A46 (Fig. 2A). In addition, direct activation of AMPK with AICAR had no effect on SLC25A46 phosphorylation (Fig. 2A). Furthermore, pharmacological stimulation with 991 activated AMPK (phosphorylation

of T172) without modifying the phosphorylation status of SLC25A46<sub>T44/T45</sub> in low-glucose conditions, nor did this treatment prevent its glucose-induced dephosphorylation (Fig. 2B). Collectively, we conclude that AMPK activity does not influence glucose-dependent SLC25A46<sub>T44/T45</sub> phosphorylation.

Interestingly, removal of extracellular Ca<sup>2+</sup> to prevent glucose-dependent Ca<sup>2+</sup> influx blocked glucose-dependent SLC25A46<sub>T44/T45</sub> dephosphorylation (Fig. 2C) suggesting the involvement of a Ca<sup>2+</sup>-sensitive kinase or phosphatase. A candidate Ca<sup>2+</sup>-regulated

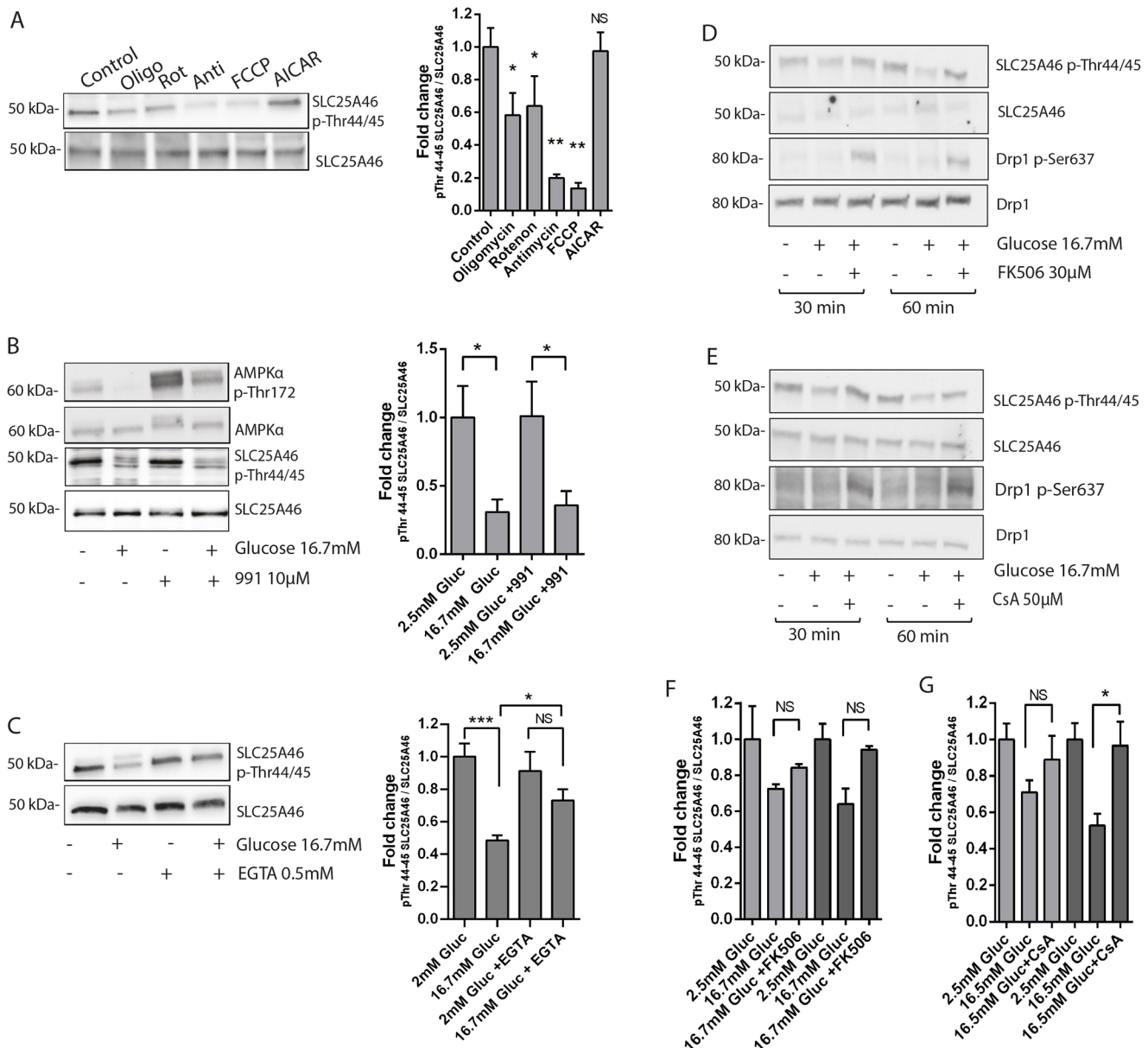


**Fig. 2. Effect of calcineurin inhibitors on glucose-dependent dephosphorylation of SLC25A46<sup>T44/T45</sup>.** Phosphorylation status of SLC25A46 was assessed with an antibody raised against the peptide phosphorylated on both T44 and T45 (upper blots). For comparison, SLC25A46 expression was revealed with an antibody against total SLC25A46 (lower blots). (A) Effect of the mitochondrial inhibitors oligomycin (2.5 μg/ml), rotenone (1 μM), antimycin A (1 μg/ml), FCCP (1 μM) and the AMPK activator AICAR (500 μM) on SLC25A46<sup>T44/T45</sup> phosphorylation. Bar graph shows mean±s.e.m. of six independent experiments (*n*=6). (B) Effect of glucose stimulation and AMPK activation with 991 (10 μM) on AMPK T172 and SLC25A46<sup>T44/T45</sup> phosphorylation. Cells were exposed to glucose for 60 min. Bar graph shows mean±s.e.m. of four independent experiments (*n*=4). (C) Glucose-dependent dephosphorylation of SLC25A46<sup>T44/T45</sup> is blocked after removal of extracellular calcium with EGTA (0.5 mM). Cells were exposed to glucose for 60 min. Bar graph shows mean±s.e.m. of six independent experiments (*n*=6). (D) Effect of the calcineurin inhibitor FK506 (30 μM) on SLC25A46<sup>T44/T45</sup> and Drp1<sup>S637</sup> phosphorylation in INS-1E cells exposed for 30 and 60 min to 16.7 mM glucose (quantification displayed in F). (E) Effect of the calcineurin inhibitor cyclosporin A (CsA; 50 μM) on SLC25A46<sup>T44/T45</sup> and Drp1<sup>S637</sup> phosphorylation in INS-1E cells exposed for 30 and 60 min to 16.7 mM glucose (quantification displayed in G). (F) Bar graph showing the effect of the calcineurin inhibitor FK506 (30 μM) on SLC25A46<sup>T44/T45</sup> and Drp1<sup>S637</sup> phosphorylation in INS-1E cells exposed for 30 (gray bars) and 60 min (dark gray bars) to 16.7 mM glucose. Mean±s.e.m. of four independent experiments (*n*=4). (G) Bar graph shows effect of the calcineurin inhibitor Cyclosporin A (CsA; 50 μM) on SLC25A46<sup>T44/T45</sup> and Drp1<sup>S637</sup> phosphorylation in INS-1E cells exposed for 30 (gray bars) and 60 min (dark gray bars) to 16.7 mM glucose. Mean±s.e.m. of four independent experiments (*n*=4). NS, not significant; \**P*<0.05; \*\**P*<0.01; \*\*\**P*<0.001 (one-way ANOVA with Tukey post-hoc test).

phosphatase affecting β-cell function is calcineurin. The two calcineurin inhibitors CsA (Fig. 2E,G) and FK506 (Fig. 2D–F) partially inhibited glucose-induced SLC25A46<sup>T44/T45</sup> dephosphorylation both at 30 and 60 min. Quantification of four independent experiments showed that, on average, both inhibitors counteract glucose-induced phosphorylation (Fig. 2F,G). Owing to the variability

between experiments, statistical significance was reached only for the condition where CsA was used for 60 min. For the shorter time-point or the FK506 treatment only a trend to inhibit glucose-dependent phosphorylation was observed. These findings suggest the Ca<sup>2+</sup>-sensitive phosphatase calcineurin might be involved in glucose-dependent regulation of SLC25A46<sup>T44/T45</sup>. In parallel, we followed

S637 phosphorylation of Drp1, a well-characterized calcineurin substrate. Glucose stimulation failed to induce Drp1<sub>S637</sub> dephosphorylation. However, both calcineurin inhibitors enhanced Drp1<sub>S637</sub> phosphorylation, confirming effective pharmacological inhibition of calcineurin in these experiments (Fig. 2D,E; quantification in Fig. S1A,B).

### **SLC25A46 overexpression lowers glucose-induced respiration and insulin secretion**

Next, we assessed the impact of SLC25A46 on mitochondrial function and its role in metabolism–secretion coupling. To this end, we disrupted SLC25A46 in INS-1E cells by Crispr/Cas9 gene targeting. Successful disruption of the *Slc25a46* alleles in individual clones was confirmed by sequencing (Fig. S2). At the protein level, SLC25A46 expression was either dramatically reduced or completely absent (Fig. 3A).

The SLC25A46-deficient cell lines had no consistent respiratory defect (Fig. 3B–D). Basal respiration (Fig. 3C) and oligomycin-dependent respiration after glucose stimulation were close to normal (Fig. 3D). Glucose- and KCl-induced cytosolic Ca<sup>2+</sup> signaling was indistinguishable between SLC25A46-deficient and wild-type INS-1E cells (Fig. 3E,F). Characterization of SLC25A46-deficient cells revealed clone-specific differences in insulin content (Fig. 3G) but insulin secretion when expressed per insulin content was close to normal. The level of glucose-stimulated insulin secretion was similar in wild-type and SLC25A46-deficient INS-1E clones (Fig. 3H). These findings showed that disruption of the *Slc25a46* gene does not markedly affect metabolism–secretion coupling in INS-1E cells.

We next tested whether overexpression of SLC25A46 had an impact on metabolism–secretion coupling. Overexpression in INS-1E cells was achieved by infecting cells with an adenovirus carrying a DDK-tagged SLC25A46 expressed under the control of the CMV promoter (Ad-CMV-SLC25A46-DDK). We obtained INS-1E cells expressing SLC25A46–DDK protein at levels that were several fold over the endogenous SLC25A46 protein levels in a manner that was dependent on the Ad-CMV-SLC25A46-DDK titer (Fig. 3I). SLC25A46 overexpression reduced basal respiration and the oligomycin-dependent fraction of glucose-induced respiration compared to control Ad-CMV-luciferase infected cells, (Fig. 3J–L). In agreement with the respiratory defect observed, glucose-induced cytosolic Ca<sup>2+</sup> signaling was significantly diminished in SLC25A46–DDK overexpressing cells (Fig. 3M,N). SLC25A46–DDK overexpression did not affect the insulin content but significantly lowered glucose-stimulated insulin secretion (Fig. 3O,P). We conclude that enhanced SLC25A46 function partially disrupts metabolism–secretion coupling in INS-1E cells.

### **SLC25A46 regulates mitochondrial dynamics in pancreatic $\beta$ -cells**

In agreement with earlier publications (Abrams et al., 2015), we found that SLC25A46 localizes to mitochondria. After differential centrifugation, SLC25A46 was enriched in the mitochondrial fraction together with TOM20 a subunit of the mitochondrial protein import machinery (Fig. 4A). In addition, we observed colocalization of SLC25A46–GFP with the mitochondrial membrane potential sensor TMRM (Fig. 4B). TMRM staining also revealed that mitochondria in INS-1E cells expressing SLC25A46–GFP were more fragmented (Fig. 4B, right panel) than in neighboring non-transfected control cells. This effect on mitochondrial morphology is consistent with earlier reports that demonstrate that SLC25A46 promotes mitochondrial fission (Abrams et al., 2015).

We therefore tested whether manipulation of SLC25A46 expression affects mitochondrial network dynamics in insulin-secreting cells. Mitochondrial morphology was inspected in control INS-1E, SLC25A46-deficient and SLC25A46 overexpressing cells and classified as hyperfused, intermediate or fragmented (Fig. 4C). In SLC25A46-deficient cells, the fraction of cells with hyperfused mitochondria was strongly increased (Fig. 4C). In INS-1E cells overexpressing SLC25A46 almost no hyperfused mitochondria were detected and a fragmented mitochondrial phenotype was observed in the majority of cells (Fig. 4C).

Mitochondrial dynamics in INS-1E cells was also studied quantitatively by fluorescence recovery after photobleaching (FRAP) using a mitochondrial matrix-targeted RFP (Fig. 4D). FRAP kinetics is known to be faster in hyperfused mitochondrial networks where recovery is rapid due to the refilling of the matrix space by RFP protein diffusion from neighboring unbleached mitochondrial filaments; when the mitochondrial network is fragmented recovery of fluorescence is slower (Mittra and Lippincott-Schwartz, 2010). SLC25A46 deficiency promoted faster and more substantial recovery after photobleaching (Fig. 4E,F), whereas overexpression of SLC25A46 precluded efficient recovery (Fig. 4E,F). Both deletion and overexpression of SLC25A46 had dramatic effects on mitochondrial morphology in INS-1E cells (Fig. 4G). Qualitative assessment of electron microscopy images did not reveal any striking phenotype beyond a slight enlargement of SLC25A46-deficient mitochondria, with no apparent effect on cristae number, density or organization in cells lacking or overexpressing SLC25A46 (Fig. 4H).

The molecular mechanism engaged by SLC25A46 to control the mitochondrial network remains poorly understood. We therefore tested whether manipulation SLC25A46 protein levels affected the protein levels of well-known factors of the core mitochondrial fission fusion machinery. We find normal protein expression of L-Opa1, S-Opa1, Drp1 and Mfn2 in SLC25A46-deficient (Fig. 4I) and overexpressing cells (Fig. 4I) that is similar to that in control INS-1E cells. Interestingly, Mfn1 protein levels were slightly increased in SLC25A46-deficient INS-1E cells (Fig. 4I). These findings are consistent with the earlier findings showing that pro-fusion protein Mfn1 is stabilized in cells lacking SLC25A46 (Steffen et al., 2017). Furthermore, the Drp1 S637 phosphorylation levels decreased in SLC25A46-deficient INS-1E cells (Fig. 4I).

### **T44/T45 phosphorylation inhibits SLC25A46-mediated mitochondrial fragmentation**

We next evaluated whether T44/T45 phosphorylation regulated the ability of SLC25A46 to alter mitochondrial network dynamics. To this end, wild-type SLC25A46 and a double phosphorylation deficient mutant SLC25A46 T44A/T45A (Fig. 5A) were cloned under the control of a doxycycline-inducible promoter and transfected into INS-1E clones lacking endogenous SLC25A46 expression. In these cells, SLC25A46 expression was strictly doxycycline-dependent (Fig. 5B). Close to maximal expression was achieved with 10 ng/ml of doxycycline in the medium for both the wild-type and phospho-deficient mutant protein (Fig. 5B). Glucose-dependent dephosphorylation was preserved in cells expressing the transgene under the control of the doxycycline-inducible promoter. As expected, the phosphoantibody did not recognize the SLC25A46 T44A/T45A mutant protein (Fig. 5B). Mitochondrial dynamics was further quantified by FRAP analysis of mitochondrial matrix-targeted RFP. Recovery after photobleaching was very rapid in the filamentous mitochondria of SLC25A46-deficient INS-1E cells (Fig. 5C,D). Consistent with its pro-fission properties, doxycycline-induced

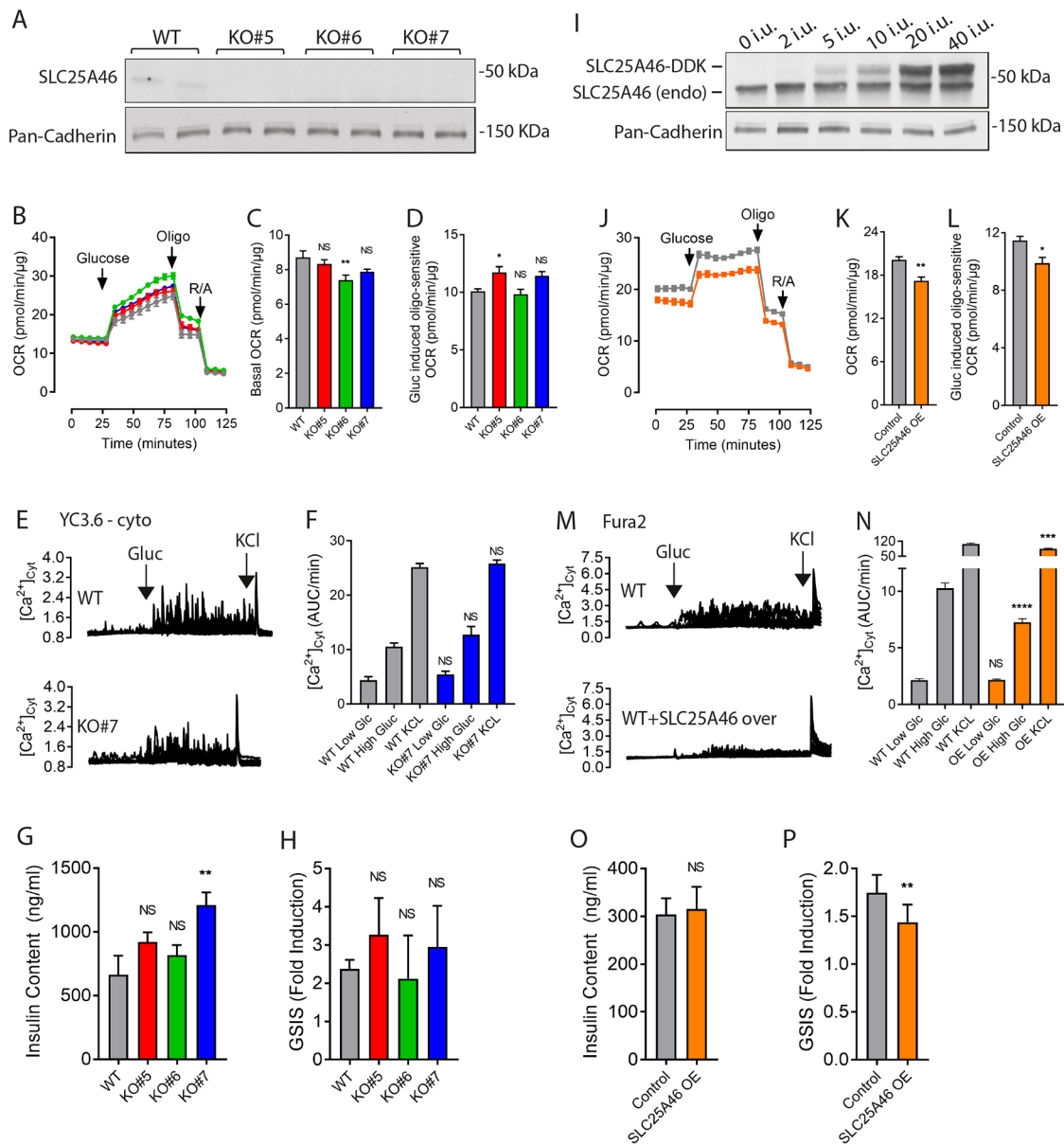


**Fig. 3. Effect of SLC25A46 protein levels on mitochondrial function and metabolism-secretion coupling in INS-1E cells.** (A) SLC25A46 protein expression in wild-type (WT) and three different SLC25A46-deficient INS-1E cell clones (KO#5, KO#6, KO#7) after knockout of the gene by Crispr/Cas9. Pan-cadherin detection was used as a loading control. (B) Effect of glucose (16.7 mM), oligomycin (Oligo, 2.5 µg/ml) and rotenone/antimycin (R/A, 1 µM/1 µg/ml) on oxygen consumption rates in wild-type and SLC25A46-deficient clones. (C) Effect of SLC25A46 suppression on basal respiration. (D) Effect of SLC25A46 suppression on glucose-induced oligomycin dependent oxygen consumption rates. For C and D, results are mean±s.e.m. from three independent experiments performed in quadruplicate. (E,F) Glucose-induced cytosolic Ca<sup>2+</sup> signaling measured with the genetically encoded Ca<sup>2+</sup> sensor YC3.6. (E) Several control INS-1E cells (upper trace) or cells lacking SLC25A46 expression (lower trace) responding to glucose (Gluc 16.7 mM) and KCl (30 mM) are shown. (F) Quantification of the area under curve of Ca<sup>2+</sup> responses in control (gray bars) and SLC25A46-deficient INS-1E cells (blue bars). Mean±s.e.m. of three independent experiments performed in quadruplicate. Total of 30 cells per condition analyzed. (G) Effect of SLC25A46 suppression on insulin content. (H) Effect of SLC25A46 suppression on the fold induction of insulin secretion when raising glucose from 2.5 to 16.7 mM. For G and H, results are mean±s.e.m. of three independent experiments performed in quadruplicate. (I) Western blot showing endogenous SLC25A46 (lower band) and DDK-SLC25A46 (upper band) expression in INS-1E cells infected with increasing number of particles of adeno-associated virus for the overexpression (OE) of DDK-SLC25A46 (i.u. refers to infection units/cell). (J) Effect of glucose (16.7 mM), oligomycin (2.5 µg/ml) and rotenone/antimycin (1 µM/1 µg/ml) on oxygen consumption rate in wild-type and SLC25A46 overexpressing cells. (K,L) Effect of SLC25A46 overexpression on basal respiration (K), and on glucose-induced oligomycin sensitive respiration (L). Mean±s.e.m. from three independent experiments performed in quadruplicate. (M,N) Effect of SLC25A46 overexpression on glucose-induced cytosolic Ca<sup>2+</sup> signaling measured with Fura-2. Quantification of area under the curve of Ca<sup>2+</sup> signals in response to glucose (16.7 mM) and KCl (30 mM) in control (gray bars) and DDK-SLC25A46 transgene expressing cells. (O,P) Effect of SLC25A46 overexpression on insulin content (O) and fold glucose-induced insulin secretion (P). Mean±s.e.m. of three independent experiments performed in quadruplicate. Blots shown in A and I are representative of three repeats. NS, not significant; \*P<0.05; \*\*P<0.01; \*\*\*P<0.001; \*\*\*\*P<0.0001 (two-tailed unpaired t-test).

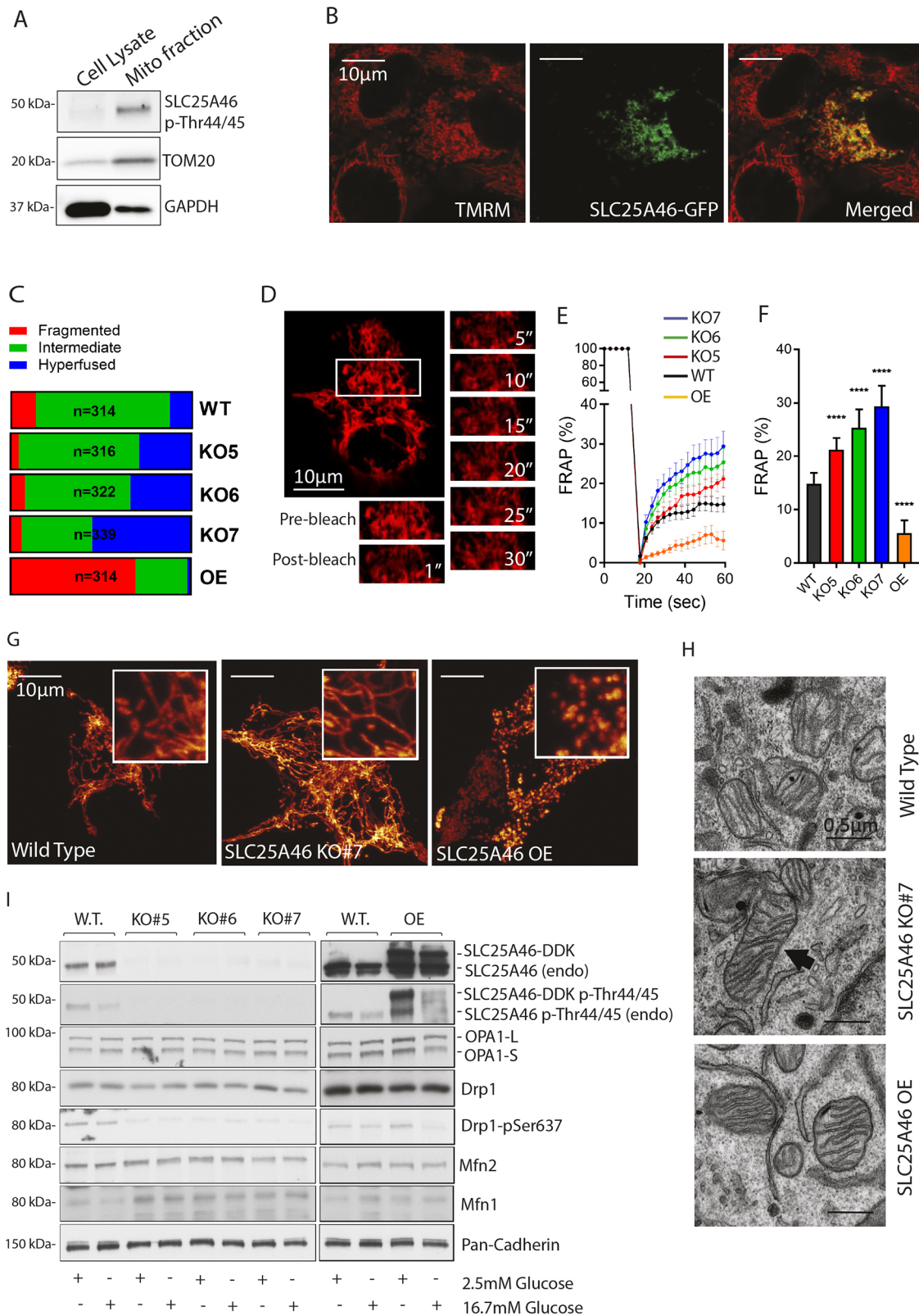


Fig. 4. See next page for legend.

expression of the wild-type protein in SLC25A46-deficient cells caused fragmentation of the mitochondrial network, slowed recovery in FRAP experiments (Fig. 5C) and provided a less pronounced recovery of the initial signal before photobleaching (Fig. 5D).

Expression of the T44A/T45A phosphorylation deficient mutant resulted in an intermediate phenotype (Fig. 5D,E). Fragmentation was less pronounced and FRAP was accelerated compared to cells expressing the SLC25A46 wild-type protein (Fig. 5C,D). We

**Fig. 4. Manipulation of SLC25A46 expression alters mitochondrial dynamics in INS-1E cells.** (A) Expression of SLC25A46 in total cell lysate and the mitochondrial fraction. For comparison the western blots were also probed for the outer mitochondrial membrane protein TOM20. (B) Confocal image of GFP-tagged SLC25A46 (green; middle) and the mitochondrial dye TMRM (red; left) and the merge (yellow; right). Images representative of four repeats. Scale bars: 10  $\mu$ m. (C) Effect of SLC25A46 suppression (KO5, KO6 and KO7) and overexpression (OE) on the percentage of cells displaying fragmented, intermediary or hyperfused mitochondria. (D) Images showing a typical FRAP assay in INS-1E cells expressing mitochondrially targeted RFP. (E,F) Fluorescence recovery after photobleaching (E) and fluorescence levels in the bleached area 60 s after the pulse (F) in wild-type (WT; black), in SLC25A46-deficient clones [KO5 (red), KO6 (green), KO7 (blue)] and SLC25A46 overexpressing cells (OE; orange). Mean $\pm$ s.e.m.; >20 cells analyzed from three independent experiments. \*\*\*\* $P$ <0.001 (two-tailed unpaired  $t$ -test). (G) Representative images of four repeats showing mitochondrially targeted RFP in wild-type, SLC25A46-deficient cells (KO#7) and SLC25A46 overexpressing cells (OE). (H) Representative electron microscopy images of the mitochondria ultrastructure in wild type, SLC25A47 deficient (KO#7) and SLC25A46 overexpressing cells. The arrow highlights a mitochondrion. Images representative of ten repeats. Scale bars: 0.5  $\mu$ m. (I) Western blot analysis of core mitochondrial shaping proteins in wild type (W.T.), SLC25A46-deficient cells (KO#7) and SLC25A46 overexpressing cells (OE), under basal conditions (2.5 mM glucose) and after short-term glucose (16.7 mM) stimulation. Western blots shown in A and I are representative of three different biological replicates.

conclude that phosphorylation of T44/T45 is required for maximal pro-fission activity of SLC25A46 and propose that T44/T45 phosphorylation regulates SLC25A46 function.

Considering the significant effect of SLC25A46 deficiency on Mfn1 levels and Drp1 S637 phosphorylation status, we further explored whether the pro-fusion properties of the phosphorylation-deficient mutant SLC25A46 T44A/T45A is concomitant with changes on these proteins. However, reintroduction of either

wild-type or double phosphorylation deficient mutant SLC25A46 T44A/T45A variants in SLC25A46-deficient cells neither modified the Mfn1 levels nor the Drp1 S637 phosphorylation status (Fig. S3).

### SLC25A46 knockout prevents palmitate-induced fragmentation but sensitizes INS-1E cells to palmitate-induced apoptosis

Shifting the balance towards mitochondrial fusion has been found previously to protect pancreatic  $\beta$ -cells from nutrient overload-induced cell death (Molina et al., 2009). Consistent with this previous report, we observed massive mitochondrial fragmentation following acute palmitate (200  $\mu$ M) stimulation of INS-1E cells (Fig. 6A). In SLC25A46-deficient cells, mitochondrial morphology underwent palmitate-induced qualitative changes, but mitochondria remained mostly hyperfused (Fig. 6A,B). Palmitate-induced fragmentation slowed the kinetics of FRAP in wild-type and SLC25A46-deficient cells. In the SLC25A46-deficient cells, FRAP remained more rapid even in palmitate-treated cells when compared to wild-type cells under control nutrient conditions (Fig. 6B). These FRAP results are consistent with the well preserved filamentous mitochondrial network of SLC25A46 deficient cells even after treatment with palmitate (Fig. 6A,B). We therefore tested whether prevention of mitochondrial fragmentation in SLC25A46-deficient cells might protect cells from palmitate-induced apoptosis in a similar manner. Cell death was followed continuously by surface labeling with Annexin V. During apoptosis, phosphatidylserine molecules translocate to the outer leaflet of the plasma membrane, which can then be detected with fluorescently labeled Annexin V (see Materials and Methods). Exposure of control INS-1E cells to palmitate induced a gradual increase in apoptosis beyond 24 h of incubation in the presence 200  $\mu$ M of the fatty acid. Apoptosis was

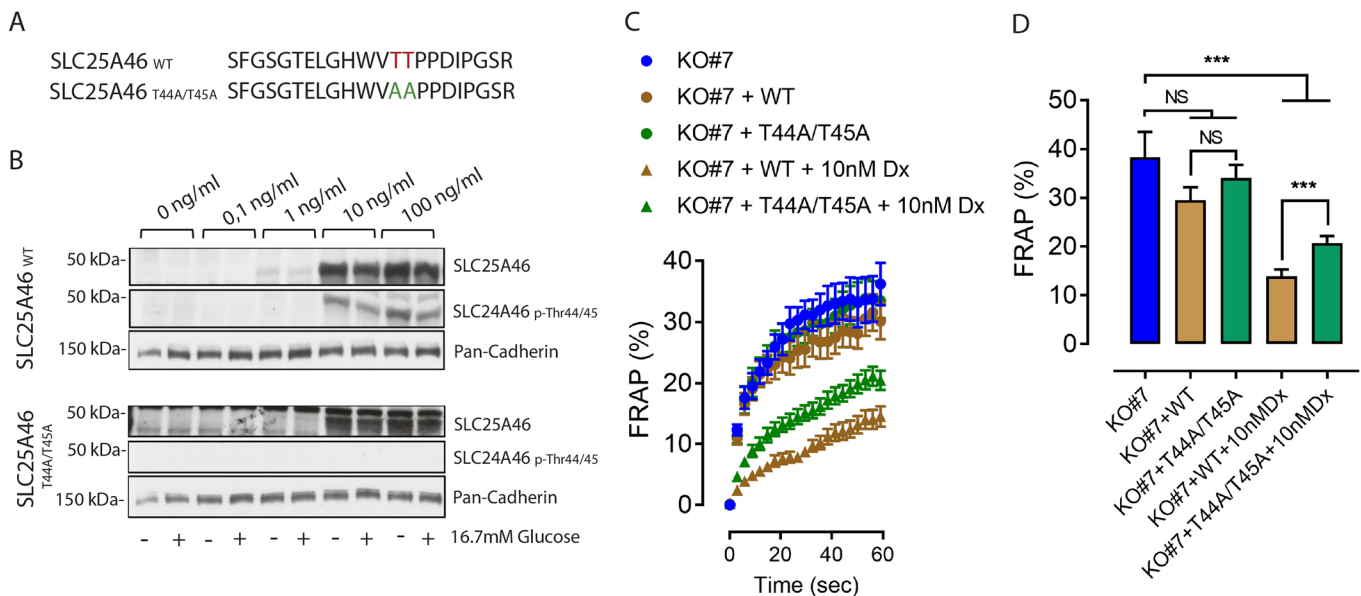


**Fig. 5. Less pronounced mitochondrial fragmentation following overexpression of an SLC25A46 phosphorylation-deficient mutant.** (A) Peptide sequences of wild-type (WT) and phospho-null variants (SLC25A46 T44A/45A). (B) Western blot showing doxycycline-induced expression of wild-type and phospho-null variant at different concentrations of doxycycline in the INS-1E cell KO7 clone. Western blots shown is representative of four repeats. (C) Kinetics of fluorescence recovery after photobleaching in INS-1E KO7 cells (blue) with and without transfection of transgenes indicated in the legend. Control conditions without induction of transgenes (circles). Induction of transgenes with doxycycline (10 nM; triangles). SLC25A46 encoding (brown) and A44/A45 mutant (green) are transfected. Mean $\pm$ s.e.m. ( $n$ =30–40 independent experiments per experimental condition). (D) Fluorescence levels in the bleached area 60 s after the bleaching pulse. Mean $\pm$ s.e.m. from 30–40 independent experiments per experimental condition. Color code as in C. NS, not significant; \*\*\* $P$ <0.001; NS, not significant (one-way ANOVA with Tukey post-hoc test).



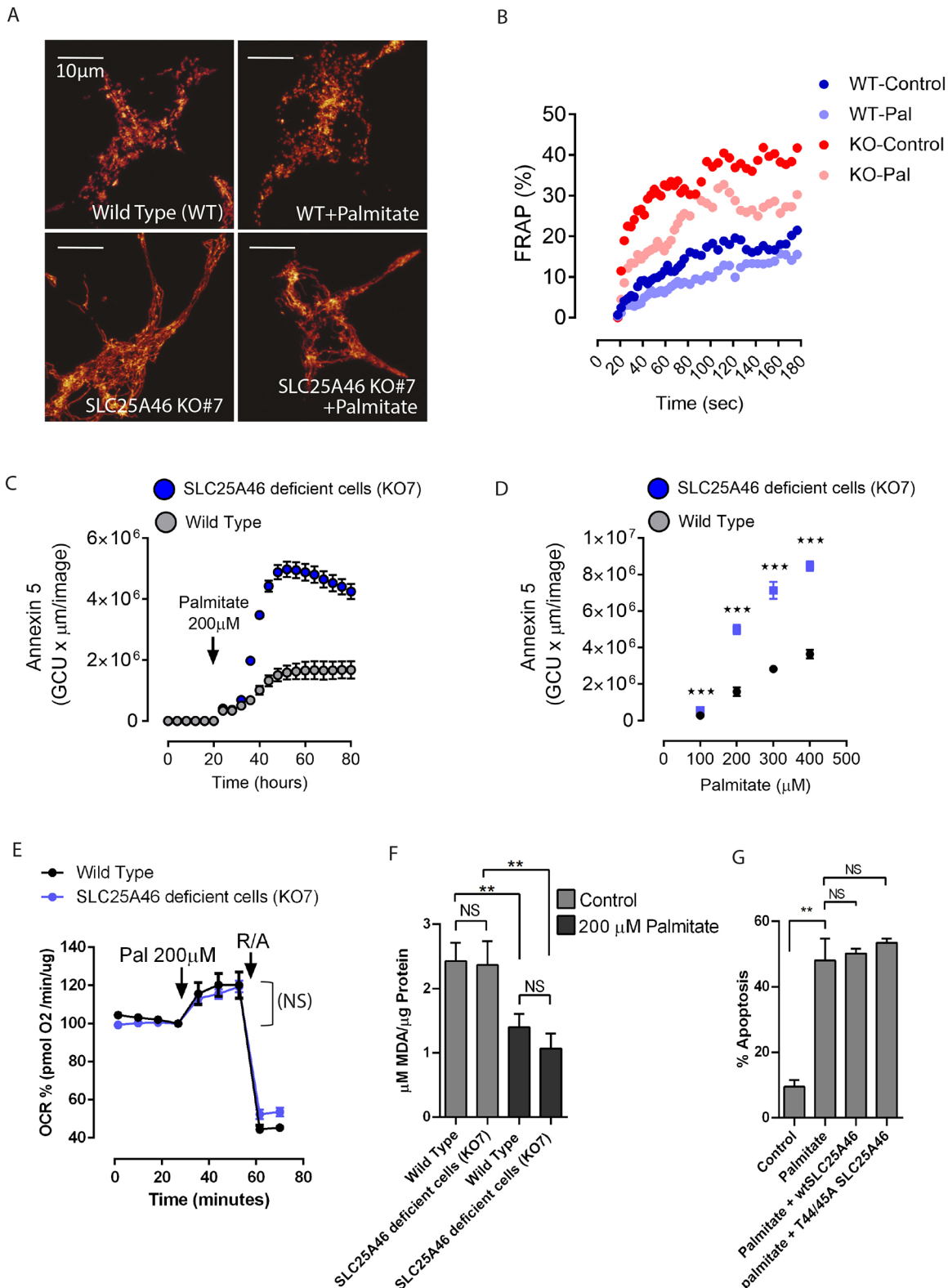


Fig. 6. See next page for legend.

highly exacerbated in SLC25A46-deficient cells (Fig. 6C). Dose-response experiments confirmed SLC25A46-deficient cells were more sensitive to palmitate-induced apoptosis over a range of palmitate concentrations (Fig. 6D). We found that insulin-secreting cells lacking SLC25A46 preserve a filamentous mitochondrial

network when challenged with palmitate. However, this ability to prevent mitochondrial fragmentation does not protect from palmitate-induced apoptosis. By contrast, INS-1E cells deficient for SLC25A46 are much more sensitive to the harmful effects of palmitate stress.

**Fig. 6. SLC25A46 deficient cells are highly sensitive to palmitate-induced apoptosis.** (A) Representative images from four repeats of the mitochondrial networks of cells expressing a mitochondrial-targeted RFP in wild-type and SLC25A46-deficient cells (KO#7) treated with and without 200  $\mu$ M palmitate. (B) Kinetics of FRAP recovery in cells expressing a mitochondrial-targeted RFP for wild-type (blue) and SLC25A46-deficient cells (KO#7; red) treated with or without 200  $\mu$ M palmitate. The paler colors are the conditions treated with palmitate for 24 h before initiation of the experiment. (C) Effect of 200  $\mu$ M palmitate on apoptosis revealed by Annexin V staining overtime in wild-type (gray circles) and SLC25A46-deficient cells (KO#7; blue circles). Shown is the mean  $\pm$  s.e.m of six measurements from a single experiment. (D) Dose-response of palmitate on Annexin V staining after 48 h palmitate incubation of wild-type (black circles) and SLC25A46-deficient cells (KO#7; blue squares). Mean  $\pm$  s.e.m of three independent experiments. (E) Effect of palmitate (Pal, 200  $\mu$ M), and rotenone/antimycin (R/A, 1  $\mu$ M/1  $\mu$ g/ml) on oxygen consumption rates in wild-type and SLC25A46-deficient cells. Mean  $\pm$  s.e.m. from three independent experiments performed in quadruplicate. (F) Levels of lipid peroxidation in wild-type and SLC25A46-deficient cells incubated either in regular cell culture medium conditions or under the same regular control condition but supplemented with palmitate 200  $\mu$ M for 48 h. Mean  $\pm$  s.e.m. ( $n=3$ ). (G) Effect of 200  $\mu$ M palmitate on apoptosis revealed by Annexin V, in control cells or expressing either wild type SLC25A46 or the phospho-null variant (SLC25A46 T44/45A). Mean  $\pm$  s.e.m. ( $n=3$ ). NS, not significant; \*\* $P<0.01$ ; \*\*\* $P<0.001$  (one-way ANOVA with Tukey post-hoc test).

To further explore the potential cellular mechanisms mediating the higher sensitivity of SLC25A46-deficient cells to palmitate-induced apoptosis, and considering previous studies reporting altered mitochondrial lipid homeostasis (Janer et al., 2016), we hypothesized that sensitivity of SLC25A46-deficient cells to palmitate-induced apoptosis might be caused by inefficient oxidation of fatty acids. To test this possibility, we measured palmitate-induced mitochondrial respiration in wild-type and SLC25A46-deficient cells (Fig. 6E). We did not find differences in the ability of SLC25A46-deficient cells and control cells to oxidize palmitate.

Lipid peroxidation plays a critical role in apoptotic cell death. We therefore tested whether lipid peroxidation was altered in cells lacking SLC25A46 expression. We observed that lipid peroxidation was not significantly different between wild-type and SLC25A46-knockout INS-1E cells (Fig. 6F). Palmitate treatment caused a marked reduction of lipid peroxidation in INS-1E control and knockout cells. The observed difference in apoptosis is therefore not due to differences in lipid peroxidation.

Considering the higher sensitivity of SLC25A46-deficient cells to palmitate-induced apoptosis, we tested whether the SLC25A46 44T/45T phosphorylation status alters the sensitivity of INS-1E cells to palmitate-induced apoptosis. Neither overexpression of wild-type SLC25A46 nor the SLC25A46 phosphorylation mutant (both T44 and T45 mutated to alanine; T44/45A) was able to prevent palmitate-induced apoptosis in INS-1E cells (Fig. 6G). We conclude that physiological levels of the SLC25A46 protein are required to protect INS-1E cells from palmitate stress. Furthermore, we tested whether, similar to glucose, palmitate was able to modify the phosphorylation status of SLC25A46. We observe that SLC25A46 levels and T44/T45 phosphorylation status remained unchanged after acute or chronic incubation with 200  $\mu$ M palmitate (Fig. S4A,B). Changes in SLC25A46 T44/T45 phosphorylation are not required for palmitate to induce INS-1E cell apoptosis.

## DISCUSSION

SLC25A46 was discovered a few years ago as mutated in individuals with a novel form of mitochondrial disease primarily affecting neuronal tissues (Abrams et al., 2015). Neuronal defects

associated with SLC25A46 loss of function include peripheral neuropathy, optic atrophy and cerebellar ataxia (Abrams et al., 2018). Unlike, most other mitochondrial membrane proteins of the SLC25 family, SLC25A46 localizes to the outer mitochondrial where it might act as a functional homolog of Ugo1p, which coordinates the fusion of the inner and outer mitochondrial membrane in yeast (Abrams et al., 2015; Sesaki and Jensen, 2004). In addition, SLC25A46, like Ugo1p, interacts both with OPA1 and mitofusin (Janer et al., 2016). Such protein-protein interaction and the shared phenotype of SLC25A46 and Opa1 mutations (i.e. both cause optic atrophy) strongly suggest that the main function of SLC25A46 is related to the control of mitochondrial morphology. However, earlier findings indicate multiple additional functions of SLC25A46 at the interface between the outer and inner mitochondrial membrane. SLC25A46 binds to proteins of the MICOS complex, which controls mitochondrial inner membrane architecture (Kozjak-Pavlovic, 2017; Neupert, 2012). As a result, impaired SLC25A46 function perturbs cristae morphology and reduces respiration (Abrams et al., 2015; Janer et al., 2016). Furthermore, SLC25A46 appears to play an important role in the exchange of phospholipids between the endoplasmic reticulum and mitochondria (Janer et al., 2016). Today many open questions regarding the molecular function of SLC25A46 remain.

We identified SLC25A46 as a phosphoprotein during a search for downstream effectors of glucose signaling in  $\beta$ -cells. Glucose-dependent phosphorylation occurs on the N-terminus in a peptide sequence preceding the first of the six transmembrane domains. Using antibodies specifically recognizing the phosphorylated epitope, we could confirm glucose dependent phosphorylation of a central pair of threonine residues (T44/T45) on this protein. SLC25A46 T44/T45 phosphorylation was most pronounced when INS-1E cells were kept under resting glucose conditions. Stimulatory glucose concentrations strongly reduced SLC25A46 T44/T45 phosphorylation. It is worth mentioning that the phosphorylation status of SLC25A46 T44/T45 slightly increased overtime regardless of glucose levels (see the time courses under low-glucose conditions and under stimulatory glucose conditions, Fig. 1F). This is probably reflecting the activity of phosphorylation pathways that still adapts to the switch from regular cell culture medium to Krebs-Ringer bicarbonate buffer HEPES (KRBH), and suggests that the phosphorylation status of SLC25A46 T44/T45 is additionally controlled by glucose-independent mechanisms.

The localization of SLC25A46 in the outer mitochondrial membrane (Abrams et al., 2015; Janer et al., 2016) renders this protein accessible to cytosolic kinases and phosphatases. Exposure of the N-terminus to the cytosol has not yet been demonstrated experimentally but was inferred from sequence comparison with two other SLC25 family members on the outer mitochondrial membrane (Palmieri, 2013; Ruprecht and Kunji, 2020; Sesaki and Jensen, 2001). We propose that SLC25A46 is a sensor of glucose-dependent signal transduction residing on the outer mitochondrial membrane in pancreatic  $\beta$ -cells. Given the essential roles mitochondria play in  $\beta$ -cell nutrient sensing and insulin secretion, a role for SLC25A46 in  $\beta$ -cell function or health is likely.

The SLC25A46 sequence surrounding T44 and T45 does not contain any typical kinase consensus sequence and we have failed to identify upstream kinases responsible for SLC25A46 phosphorylation. On the other hand, we noted that blocking glucose-induced  $Ca^{2+}$  rises in INS-1E cells prevented glucose-dependent dephosphorylation of T44/T45. We find that the two calcineurin inhibitors CsA and FK506 blocked glucose-dependent

dephosphorylation of SLC25A46, consistent with earlier reports that provide strong evidence for activation of this  $\text{Ca}^{2+}$ -activated phosphatase during glucose stimulation (Jansson et al., 2008; Sreaton et al., 2004). Of note, the calcineurin substrate Drp1 (S637) was also hyperphosphorylated in the presence of either calcineurin inhibitor. In contrast to SLC25A46, Drp1 was dephosphorylated in both at low and high glucose levels. Glucose-dependent  $\text{Ca}^{2+}$  rises are therefore unlikely to affect Drp1 S637 phosphorylation and the control of mitochondrial fission via Drp1 in  $\beta$ -cells. Our results on SLC25A46 suggest that, in addition to the important role of calcineurin in linking glucose levels to proliferation and survival of  $\beta$ -cells through TORC2 and NFAT2 dephosphorylation (Heit et al., 2006; Jansson et al., 2008; Sreaton et al., 2004), calcineurin might directly influence mitochondrial function by dephosphorylating SLC25A46. We establish a new link between cytosolic  $\text{Ca}^{2+}$  signaling and the regulation of  $\beta$ -cell mitochondria.

Mitochondria in  $\beta$ -cells participate actively in nutrient sensing and generate coupling factors, most importantly ATP, that regulate insulin secretion (Wiederkehr and Wollheim, 2012). In INS-1E cells lacking SLC25A46, neither the basal respiratory rate of oxygen consumption nor the biphasic rise of glucose-dependent respiration was altered. Consistent with normal oxidative phosphorylation, our ultrastructural study of mitochondria reveals no apparent disorganization of cristae in the inner mitochondrial membrane.

The lack of respiratory phenotype in mutant insulin-secreting cells is diametrically opposite to the pronounced oxidative phosphorylation defect observed in SLC25A46 mutant neurons or patient fibroblasts carrying SLC25A46 mutations (Abrams et al., 2015; Janer et al., 2016; Wan et al., 2016). In these cell types, the absence of SLC25A46 function also causes pronounced alterations of mitochondrial ultrastructure, most importantly a disruption of cristae organization. Of note, we identify significant variability in the respiratory activity of the different clones (Fig. 3). We cannot rule out off-targeting edition events in our Crispr/Cas-edited cell clones, as the genomes of the three clones were not fully sequenced.

Glucose-induced cytosolic  $\text{Ca}^{2+}$  signaling was also normal in INS-1E SLC25A46 knockout cells. This is another strong argument for close to normal respiratory function. Strong impairment of mitochondria respiration such as observed in mutant neurons and fibroblasts would have prevented glucose-induced ATP production and consequently  $\text{Ca}^{2+}$  influx linked to plasma membrane electrical activity in  $\beta$ -cells. Given the normal cytosolic  $\text{Ca}^{2+}$  signals, it is not surprising that glucose-induced insulin secretion was also preserved in SLC25A46 mutant INS-1E cells. We propose that mitochondria in INS-1E express proteins compensating for the loss of SLC25A46 function.

Based on our findings in INS-1E knockout cells, we cannot rule out that SLC25A46 dysfunction impacts oxidative phosphorylation and thereby metabolism–secretion coupling in primary pancreatic  $\beta$ -cells. Indeed, a possible role for SLC25A46 in primary  $\beta$ -cells *in vivo* has recently been suggested through the careful genetic and phenotypic analysis of the insulin hyposecretion mouse (ihs) (Nakano et al., 2020). The authors identified *Slc25a46* as one of a small group of genes that could be responsible for the described severe insulin secretion defect in these mice.

We demonstrate mild mitochondrial impairment in insulin-secreting cells overexpressing SLC25A46. Both basal respiration and ATP-synthase dependent respiration were reduced in cells overexpressing the transgene. The mitochondrial defect in these cells is likely responsible for the strongly impaired cytosolic  $\text{Ca}^{2+}$  signaling and the observed reduced glucose-induced insulin

secretion. We conclude that SLC25A46 overexpression interferes with the endogenous protein carrying out its function. A possible mechanistic explanation is that SLC25A46, when overexpressed, titrates out some of its interaction partners preventing their normal assembly into functional units. Such a dominant-negative effect might also be experienced by cells expressing point mutations of SLC25A46 in cells from individuals with mitochondrial disease.

In pancreatic  $\beta$ -cells, mitochondria form a dense cortical filamentous network in close proximity with the plasma membrane. Mitochondria are therefore positioned strategically to sense glucose-induced  $\text{Ca}^{2+}$  influx and locally generate coupling factors close to insulin granule to promote their mobilization and exocytosis. Mitochondrial filaments in INS-1E and primary  $\beta$ -cells on average are rather short and highly dynamic. The most striking phenotype of SLC25A46 knockout INS-1E cells is the dramatic elongation of mitochondrial filaments. The mitochondrial filamentation phenotype in INS-1E cells lacking SLC25A46 is consistent with earlier findings in other cell types (Abrams et al., 2015; Janer et al., 2016; Wan et al., 2016). Surprisingly, the pronounced hyperfusion of mitochondria does not affect metabolism–secretion coupling as discussed above. This is in contrast to the hyperfusion caused by lack of Drp1 in  $\beta$ -cells, which consistently impairs glucose-induced insulin secretion *in vitro* and *in vivo* (Hennings et al., 2018; Kabra et al., 2017; Reinhardt et al., 2016).

SLC25A46 overexpression in INS-1E cells induced massive mitochondrial fragmentation, in agreement with earlier findings in fibroblasts, neurons and HeLa cells (Abrams et al., 2015; Janer et al., 2016; Wan et al., 2016). The results suggest SLC25A46 contributes as a pro-fission factor to mitochondrial dynamics, but the underlying molecular mechanisms remain elusive. In fibroblasts, it has been shown that SLC25A46 interacts with Mfn1, Mfn2 and Opa1 core components of the mitochondrial fission machinery (Janer et al., 2016). Later, it was proposed that absence of SLC25A46 stabilized Mfn1 and Mfn2 levels as well as their mutual interaction, favoring pro-fusion (Steffen et al., 2017). In agreement with these findings, we observe that SLC25A46 deficiency slightly increased Mfn1 levels. However, overexpression of SLC25A46 did not modify Mfn1 levels nor the abundance of other mitochondrial-shaping factors tested despite the robust fragmentation phenotype. We predict the existence of additional factors mediating the pro-fission properties of SLC25A46 beyond the regulation of Mfn1 and/or Mfn2 stability.

The massive mitochondrial fragmentation observed in SLC25A46 overexpressing insulinoma cells might explain why SLC25A46 has dominant negative effects on mitochondrial respiration and glucose-induced insulin secretion. These findings are consistent with earlier work. Pancreatic  $\beta$ -cells lacking the mitochondrial fusion proteins Opa1, Mfn1 or Mfn2 also have strongly fragmented mitochondria and impaired glucose-induced insulin secretion (Zhang et al., 2011). Massive fragmentation might be incompatible with normal metabolism–secretion coupling. Proper localization of cortical mitochondria and the regulation of mitochondrial morphology likely influence effective coupling between glucose sensing and the control of insulin secretion. Phosphorylation of SLC25A46 might influence these processes by altering mitochondrial morphology and positioning.

We tested whether the regulation of SLC25A46 phosphorylation on T44 and T45 has functional consequences. Expression of a SLC25A46 alanine mutant (T44A/T45A) that cannot be phosphorylated was much less efficient at causing mitochondrial fragmentation than expression of the corresponding wild-type

protein. These findings suggest SLC25A46 phosphorylation stimulates fission activity.  $\text{Ca}^{2+}$ -dependent SLC25A46 dephosphorylation would therefore predict a shift to more elongated mitochondria during glucose stimulation. However, we and others have not observed acute glucose-induced mitochondrial elongation in INS-1E or primary  $\beta$ -cells (data not shown; Jhun et al., 2013; Molina et al., 2009). Earlier work by Shirihai and colleagues demonstrated that neither acute nor chronic rises in glucose had a significant impact on mitochondrial morphology in insulin-secreting cells (Molina et al., 2009). These findings are incompatible with the promotion of mitochondrial fusion caused by glucose-associated  $\text{Ca}^{2+}$  rises and the dephosphorylation of SLC25A46.

Interestingly, Molina et al. found pronounced mitochondrial fission in response to palmitate or a combination of elevated glucose and palmitate. Such lipotoxic conditions have been used to mimic a diabetogenic environment to study the stressed pancreatic  $\beta$ -cell. The authors further observed that slowing fission by knocking down Fis1 prevented palmitate-induced fragmentation and importantly almost completely blocked palmitate-induced apoptosis (Molina et al., 2009). Knocking out the fission factor SLC25A46 in INS-1E cells similarly almost completely prevented palmitate-induced fragmentation. This mechanism of blocking mitochondrial fragmentation, however, did not protect INS-1E cells from palmitate-induced apoptosis. On the contrary, SLC25A46 knockout cells were much more sensitive to the toxic effects of palmitate at all concentrations tested. These observations might be linked to the altered mitochondrial phospho-lipidome reported in SLC25A46 deficient cells (Janer et al., 2016), given the modulatory effects of mitochondrial membrane lipids on mitochondrial-driven apoptosis. We conclude that maintaining the mitochondrial filamentous network is not sufficient to protect  $\beta$ -cells from lipotoxicity-induced apoptosis. More importantly, these findings suggest a crucial role for SLC25A46 in the control of mitochondria-induced apoptosis in  $\beta$ -cells.

The demonstrated role of SLC25A46 in cristae morphology in other cell types could be linked to the control of apoptosis by SLC25A46. In  $\beta$ -cells, this role for SLC25A46 in cristae morphology and function might be compensated for under normal nutrient conditions not when palmitate stress is applied. Chronic palmitate treatment is known to promote mitochondrial cytochrome *c* release in  $\beta$ -cells (Maedler et al., 2001; Molina et al., 2009). The inability to maintain intact cristae structures under nutrient stress conditions in SLC25A46 mutant  $\beta$ -cells might favor cytochrome *c* release during palmitate-induced apoptosis. Our findings show that although there are compensatory mechanisms preventing the induction of apoptosis, absence of this protein on the outer mitochondrial membrane dramatically sensitizes insulin-secreting cells to nutrient stress.

In summary, we identified SLC25A46 as a novel downstream effector of glucose-induced  $\text{Ca}^{2+}$  signaling in pancreatic  $\beta$ -cells. This protein plays a central role in the control of mitochondrial fission. However, the molecular function of SLC25A46 is not likely limited to the regulation of mitochondrial dynamics. Earlier work strongly suggests its involvement in basic mitochondrial processes such as cristae morphology and respiratory activity. SLC25A46 mutant insulin-secreting cells are unremarkable in this respect as they respire normally and are able to perform all aspects of metabolism secretion coupling, which are known to depend on mitochondrial function. Importantly, we observe that insulin-secreting cells lacking SLC25A46 are strongly sensitized to palmitate-induced apoptosis. The possible involvement of SLC25A46 in the regulation of mitochondria and the control of apoptosis is an important topic for future research.

## MATERIALS AND METHODS

### Reagents

Oligomycin (75351), rotenone (R8875), antimycin (A8674), FCCP (C2920), HEPES (H3375), EGTA (E3889), Tris (T1503), glycine (G8898), malondialdehyde (MDA; M-012), 2-thiobarbituric acid (TBA; T5500), sucrose (S0389), HCl (H1758), SDS (L3771),  $\text{MgSO}_4$  (M7506), NaCl (S9888),  $\text{CaCl}_2$  (C1016), KCl (P3911),  $\text{NaH}_2\text{PO}_4$  (S0751), palmitic acid (P5585), bovine serum albumin (A8806), FK506 (F4679) and cyclosporin A (30024) were acquired from Sigma-Aldrich (St Louis, MO, USA). Lipofectamine 2000 (10696153) and the BCA protein assay kit (10678484) were acquired from Thermo Fisher Scientific (Waltham, MA, USA). AICAR (2840) and carbachol (2810) were acquired from Tocris Bioscience (Bristol, UK). 911 (S8654) was acquired from Selleckchem (Huston, USA). SLC25A46-Myc-DDK (RR209520, Origene), SLC25A46-tGFP (MG206612) and COX8(MTS)-RFP expressing plasmids (RC100126) were acquired from Origene (USA). The YC3.6cyto (fluorescent protein yellow cameleon version 3.6) pcDNA3 construct was kindly provided by Prof. A. Miyawaki (Riken Brain Science Institute, Wako, Japan). Other reagents and provider are indicated in the respective method section.

### INS-1E cell culture

INS-1E cells were cultured at 37°C in a humidified atmosphere (5%  $\text{CO}_2$ ) in RPMI-1640 medium (Thermo Fisher Scientific) that contained 11 mM glucose, supplemented with 10 mM HEPES (pH 7.3), 10% (v/v) heat-inactivated fetal calf serum (Chemie Brunschwig, Switzerland), 1 mM sodium pyruvate, 50  $\mu\text{M}$  2-ME, 50  $\mu\text{g}/\text{ml}$  penicillin and 100  $\mu\text{g}/\text{ml}$  streptomycin. INS-1E cells were obtained from Pierre Maechler laboratory at the University of Geneva, Switzerland, and they were recently authenticated and tested for contamination.

### Phosphoproteomic data re-analysis

Our recent study describing the phosphoproteome dynamics over the first hour of glucose stimulation in insulin secreting cells (Santo-Domingo et al., 2019) was reanalyzed in the current work with the aim to increase the chances of capturing new glucose-regulated mitochondrial phosphoproteins. Scaffold PTM (Proteome Software, Portland, OR, USA) parameters were here modified to keep all phosphorylated peptides, whatever was the modification localization probability (i.e. minimum localization probability was set to 0%). Of note, peptide SFGSGTELGHVWTTTPDIPGSR of SLC25A46 was confidently identified as di-phosphorylated but previously unreported because its phosphorylation sites were assigned with only 40% probability to S35 and T45. The newly generated protein list of glucose-regulated phosphorylated sites ( $P < 0.05$ ) was analyzed in Mitominer 4.0 (<http://mitominer.mrc-mbu.cam.ac.uk/release-4.0/begin.do>) using the IMPI database (rat mitochondrial proteome) as reference to obtain evidence of mitochondrial localization.

### Western blotting

For glucose-stimulated experiments 60-mm diameter Petri dishes were seeded with  $2 \times 10^6$  INS-1E cells, and maintained in the incubator for 48 h until they reached 70–80% confluence. The day of the experiment, INS-1E cells were equilibrated in KRBH containing 2.5 mM glucose for 30 min at 37°C. Subsequently, the plates were divided in two experimental groups and incubated either with 16.7 mM (high glucose) or maintained in 2.5 mM glucose in the same KRBH (low glucose). Cell lysis was carried out after 60 min of stimulation or at the time points indicated in the figures. Cells were lysed for 15 min on ice in RIPA buffer that was supplemented with protease inhibitors (Roche, Basel, Switzerland), phosSTOP phosphatase inhibitor cocktail (Roche), 10 mM NaF, 0.1  $\mu\text{M}$  PMSF and 2 mM Na-orthovanadate for complete phosphatase inhibition. Lysate was centrifuged at 14,000 *g* for 20 min at 4°C, and the protein content of the supernatant was determined by using Pierce BCA Protein Assay Kit (Pierce, USA). An amount of 25  $\mu\text{g}$  of total protein was loaded onto SDS-PAGE gels. For immunoblotting, proteins were transferred onto nitrocellulose membrane with i-blot (Thermo Fisher Scientific) and probed with the following antibodies: anti-SLC25A46 (12277-1-AP; Protein Tech), anti-DDK (TA50011-100; Origene), anti-AMPK $\alpha$  (#2532; Cell Signaling), anti-

AMPK $\alpha$ -pThr172 (#2535; Cell Signaling), anti-tubulin (05-829; Chemicon, Temecula, CA, USA), Anti-Drp1 (YZ6211, YenZyme Antibodies), anti-Drp1 p637 (YZ5447, YenZyme Antibodies), anti-Opal (612606; BD Biosciences), anti-Mfn1 (YZ5443; YenZyme Antibodies), anti-Mfn2 (YZ5445; YenZyme Antibodies), anti-Tom20 (Santa Cruz Biotechnology, Dallas, TX, USA), anti-pan-cadherin (#4068; Cell Signaling), anti-GAPDH (ab8245; Abcam), and anti-turboGFP (TA150041; Origene) antibodies. All antibodies were used at 1/000 dilution. Horseradish peroxidase-conjugated secondary antibodies were used, followed by chemiluminescence detection (Amersham Biosciences, Pittsburgh, PA, USA). Phospho-specific antibodies anti-Thr44 SLC25A46 and anti-Thr44/45 SLC25A46 were produced by YenZyme Antibodies (Brisbane, CA, USA). Briefly, modified (phosphorylated) peptides were synthesized. The phosphorylated peptides were conjugated to a carrier protein to render them immunogenic and two rabbits were immunized. For each antibody, the elicited antibody was affinity-purified against the same modified peptide used for immunization. Finally, purified antibody was affinity absorbed against the non-modified peptide counterpart to separate the phospho-specific antibody from the cross-reactive antibody populations. For lambda phosphatase assays, cell lysates were either mock or lambda phosphatase (P0753, New England Biolabs) treated for 60 min at 30°C with 400 U enzyme.

### INS-1E adenovirus infection

Adenoviral production was performed by Sirion Biotech (Germany). Briefly, SLC25A46-DDK and luciferase ORFs were cloned into pO6A5-CMV adenoviral shuttle vectors. CAP packaging cells were transfected and subsequently lysed to recover SLC25A46-DDK and luciferase infection particles. For the experiments, INS1E cells were infected 2 days after plating. To achieve SLC25A46 overexpression, samples were infected with 20 infection units/cell of SLC25A46-DDK adenovirus particles for 90 min in RPMI medium at 37°C. Experimental controls were infected with 20 infection units/cell of luciferase adenovirus particles. Cells were washed with phosphate-buffered saline (PBS) before adding fresh INS-1E cell culture medium. The measurements were performed 24 h after infection.

### Mutagenesis and cloning

The SLC25A46 T44/45A phospho-null mutant was generated by site-directed mutagenesis using the kit GeneArt<sup>®</sup> Site-Directed Mutagenesis PLUS (Invitrogen). The following set of oligonucleotides were used to introduce the nucleotide changes: FW, 5'-CTGGGCCACTGGGTGGCAG-CACCCCCGGACATCC-3'; RV, 5'-GGATGTCCGGGGGTGCTGCCA-CCCAGTGGCCAG-3'.

SLC25A46-wt and SLC25A46 T44/45A doxycycline-induced plasmids were generated by cloning the corresponding full cDNA sequences of both versions of the gene on Tet-On<sup>®</sup> 3G Inducible Expression System (631168, Takara).

### Oxygen consumption

Oxygen consumption in INS-1E cells was measured by using an XF96 instrument (Seahorse Bioscience, Billerica, MA, USA). INS-1E cells were seeded onto polyornithine-coated tissue culture plates (Seahorse Biosciences) at a density of 20,000 cells per well. After 2 days, INS-1E cells were washed twice and incubated in basal KRBH buffer that contained 2.5 mM glucose, 140 mM NaCl, 3.6 mM KCl, 0.5 mM NaH<sub>2</sub>PO<sub>4</sub>, 0.5 mM MgSO<sub>4</sub>, 1.5 mM CaCl<sub>2</sub>, 10 mM HEPES, and 5 mM NaHCO<sub>3</sub> (pH 7.4). Respiration rates were determined every 6 min. All experiments were performed at 37°C. Respiratory chain inhibitors were added as indicated in the figures at the following concentrations: rotenone, 1  $\mu$ M; antimycin A, 1  $\mu$ g/ml; oligomycin, 2.5  $\mu$ g/ml.

### Ca<sup>2+</sup> imaging

Cytosolic Ca<sup>2+</sup> was measured with the genetically encoded sensor YC3.6cyto or Fura2. For Ca<sup>2+</sup> measurements based on YC3.6cyto, INS-1E cells were plated on polyornithine-treated glassbottom dishes (35 mm diameter; MatTek, Ashland, MA, USA) and transfected with pcDNA3 YC3.6cyto using Jetprime transfection reagent (Polyplus-Transfection SA,

Illkirch-Graffenstaden, France). At 2 days after transfection, cells were imaged on KRBH buffer. For Fura 2 measurements, cells were incubated 40 min in KRBH buffer containing 2  $\mu$ M Fura2-AM at room temperature, followed by 30 min in KRBH. Cells were imaged on KRBH. Glass coverslips were inserted in a thermostatic chamber (Life Imaging Services, Basel, Switzerland) that was maintained at 37°C. Cells were imaged on a DMI6000 B inverted fluorescence microscope using an HCX PL APO 63 $\times$ /1.40–0.60 NA oil immersion objective (Leica Microsystems, Wetzlar, Germany) and an Evolve 512 back-illuminated charge-coupled device with 16 $\times$ 16-pixel camera (Photometrics, Tucson, AZ, USA). For YC3.6cyto measurements, cells were excited at 430 nm through a BP436/20 filter. Two emission images were acquired with BP480/40 and BP535/30 emission filters. For Fura2 measurements, cells were alternatively excited with the BP340/10 and BP387/10 filters and emission was collected with BP535/25 filter. Background was subtracted, fluorescence ratios were calculated in MetaFluor 7.0 (Meta Imaging Series; Molecular Devices, Sunnyvale, CA, USA) and analyzed in Excel (Microsoft, Redmond, WA, USA) and GraphPad Prism 5 (GraphPad Software, La Jolla, CA, USA). Images were taken every 2 s.

### Static insulin secretion

INS-1E cells were plated on a polyornithine-treated 24-well plate. After 48 h, cells were washed in KRBH, containing (in mM): 140 NaCl, 3.6 KCl, 0.5 NaH<sub>2</sub>PO<sub>4</sub>, 0.5 MgSO<sub>4</sub>, 1.5 CaCl<sub>2</sub>, 10 HEPES, 5 NaHCO<sub>3</sub>, and pH 7.4 with 2.5 mM glucose. Cells were stimulated for 30 min with 16.7 mM glucose and supernatants were collected. Cellular insulin content was extracted with a mixture of ethanol (75%) and HCl (1.5%) overnight at 4°C. Insulin was measured using a Rat Insulin Enzyme Immunoassay Kit (SpiBio, Montigny-le-Bretonneux, France).

### INS-1E SLC25A46 knockout generation

sgRNA was designed using CHOPCHOP (<https://chopchop.rc.fas.harvard.edu/>) and cloned into Cas9-sgRNA lentiviral vector (pLenti-U6-sgRNA-SFFV-Cas9-2A-Puro; abm<sup>®</sup>). The target sequence was 5'-GCGGACGG-CACACCGTACGA-3' (*Rattus norvegicus*, NM\_001100515). Lentivirus production was performed according to abm protocol as described on the website (<https://www.abmgood.com/Lentivirus-Packaging-Systems.html>). For transduction, a MOI of 5 was used to transduce 2 $\times$ 10<sup>5</sup> wild type INS-1E cells. Puromycin selection was performed two days after transduction using 1.1  $\mu$ g/ml of G264. After puromycin selection, genomic DNA was extracted for PCR. The PCR product was sequenced and compared to the reference genome. Following puromycin selection, the polyclonal pools with indels that induce frame shift mutations were selected for further expansion. Subsequently, monoclonal selection was performed via single cell dilution and cell underwent drug selection at the same time. Clones were then screened using CRISPR Genomic Cleavage Detection Kit (G932, abm) and successful clones were further submitted to Sanger Sequencing validation (forward primer sequence: 5'-GCTACGGAGAAGTACC-CAG-3' and reverse primer sequence: 5'-GTGACTCCACCTA-TAGGCGC-3'). Sequencing results showing frame-shift mutations confirmed successful genome editing (Fig. S2).

### Transmission electron microscopy sample preparation

INS-1E cells were seeded, allowed to attach on polyornithine coated coverslips (Nalge Nunc Int. #174969) and cultured for 4 days. The cells were then washed twice briefly with PBS pH 7.4 and fixed for 1 h in PBS containing 2% paraformaldehyde and 2.5% glutamine at room temperature. The cells were washed three times at 4°C in cacodylate buffer (0.1 M, pH 7.4). The samples were postfixed twice for 40 min at room temperature in cacodylate buffer (0.1 M, pH 7.4) with 1% osmium tetroxide. The cells were washed for 5 min in distilled water and stained for 40 min in 1% uranyl acetate. The cells were washed for an additional 5 min in distilled water and dehydrated in a graded alcohol series (1 $\times$ 50%, 1 $\times$ 70%, 2 $\times$ 96%, 2 $\times$ 100%). The cells were embedded in Durcupan. The samples were placed on coated glass slides and left overnight at 65°C.

### Mitochondrial isolation

INS-1E cells at ~80% confluency from two 75-cm<sup>2</sup> flasks were washed with PBS and detached by trypsinization. The cell suspension was centrifuged at

room temperature (200 g, 5 min). The cell pellet was resuspended in 1 ml of sucrose/TES buffer (300 mM sucrose, 10 mM TES, 0.5 mM EGTA, pH 7.4) and incubated for 1 h on ice. Subsequently, the cells were lysed in a glass homogenizer and centrifuged at 4°C (200 g for 10 min). The mitochondria-containing supernatant was subjected to a second centrifugation at 4°C (6000 g for 15 min). Finally, the mitochondrial containing pellet was resuspended in 100 µl of RIPA buffer for western analysis.

### Mitochondrial network connectivity

Fluorescence recovery after photobleaching (FRAP) was used to measure mitochondrial connectivity. INS-1E cells were plated on polyornithine-treated glass-bottom dishes (35 mm diameter; MatTek, Ashland, MA, USA) and transfected with mitochondrial matrix-targeted RFP (Cox8-RFP, Origene, USA) using Jetprime transfection reagent (Polyplus-Transfection SA, Illkirch-Graffenstaden, France). At 2 days after transfection cells were imaged at 37°C on a SP5 confocal microscope (Leica Microsystems, Wetzlar, Germany). Experiments and image analysis were performed using the LAS AF FRAP wizard (Leica Microsystems, Wetzlar, Germany). The mitochondrial network was imaged on the confocal microscope SP5 using a 63× objective. Samples were excited with the 561 nm laser line and emission was collected between 570–700 nm. Five images were acquired (3 images/second) before applying one single bleaching pulse (100 ms, 571 nm laser, 70% power, 7.0 width×2.0 height µm areas) followed by live imaging initially at 1 frame/second for 1 min and later at 0.2 frame/second for an additional minute to allow RFP equilibration across the lumen of the mitochondrial network. Loss of focus and movement artifacts were minimized by using a large pinhole aperture (2.00 AU). ‘Zoom in’ and ‘Set background to zero’ modes were respectively set to reduce the scan field during photobleaching and to prevent that the background outside the exposed ROI being bleached.

Representative images of mitochondrial networks were also obtained by confocal imaging. Briefly, confocal Z-stacks of cells expressing the matrix-targeted red fluorescent protein Cox8(MTS)-RFP were acquired on a SP5 confocal microscope (Leica Microsystems, Wetzlar, Germany) inverted microscope using a 63× objective, 561 nm excitation and 570–700 nm emission. 15 Z-stack images per cell were projected using the Image J tool ‘Z-projection’ to generate complete mitochondrial network images. Images of single cell mitochondrial networks were qualitatively classified by researchers who were not aware of the experimental condition as fragmented, intermediate and hyperfused (300 cells per condition; three experiments).

### Apoptosis assay

Annexin V-labelled apoptotic cells were imaged with the Incucyte ZOOM live-cell analysis system (Essen bioscience). INS-1E cells were plated at 40,000 cells/well in 96-well plates, 24 h prior to the experiments. For the assay, FITC-labeled Annexin V (Incucyte® Annexin V Green) and treatments (BSA-Palmitate and BSA) were added to the complete INS-1E growth medium according to the manufacturer’s instructions (Incucyte Zoom, Sartorius). Cells were incubated at 37°C and 5% CO<sub>2</sub> in the presence of fluorescently labeled Annexin V. Images were taken with 10× objective every 4 h (excitation, 460 nm; passband, 440–480 nm; emission, 524 nm; passband, 504–544 nm) and processed with the Incucyte Zoom software. Briefly, a training set of images including untreated and staurosporine-induced apoptosis cells was analyzed with the Incucyte ZOOM image analysis tool to establish a set of internal parameters for an image processing definition that optimally separate positive cells from background. Settings for segmentation were as follows: ‘Adaptive Background’, Threshold (GCU) ‘2.000’, Edge Split ‘off’, Edge Sensitivity ‘off’, Cleanup: Hole Fill (µm<sup>2</sup>) ‘off’ and Filters for Area, Eccentricity, mean intensity and integrated intensity, ‘off’. This set of internal parameters were subsequently applied to the whole image collection. Images were segmented and apoptosis was quantified as total integrated apoptotic intensity (GCU×µm<sup>2</sup> / image).

### Lipid peroxidation

Quantification of lipid peroxidation was carried out using the TBARS assay. INS-1E cells at ~80% confluency from 60 mm-diameter culture plates were washed with PBS and detached by trypsinization. Then, cell suspensions

were centrifuged at 200–300 g for 4 min and the pellets frozen at –80°C. After 1 h cell pellets were thawed at room temperature, resuspended in 15 µl PBS and vigorously homogenized to achieve mechanical rupture of the cells. At this point, 12 µl of the suspension was collected in a new Eppendorf for the TBARS assay (the remaining volume was transferred for BCA assay). Samples were subsequently treated with 390 µl of 0.2 M Glycine-HCl pH 3.6 buffer and 250 µl of a 0.5% TBA, 2% SDS solution and incubated at 90°C for 45 min in the absence of light. For measurements, 200 µl of each sample was transferred to a 96-well plate and read at 523 nm in a SpectraMax® ABS Plus spectrophotometer (Molecular Devices). Finally, optical density values were interpolated against a 0 to 80 µM MDA calibration curve to obtain lipid peroxides concentration as MDA concentration (in µM) and normalized by protein content.

### Statistical analysis

All statistical analyses were performed using Prism software (GraphPad). Significance between two experimental groups was determined using a two-tailed unpaired Student’s *t*-test whereas group sets were analyzed using an one-way ANOVA (post-hoc Tukey test). NS, not significant; \**P*<0.05; \*\**P*<0.01; \*\*\**P*<0.001; \*\*\*\**P*<0.0001.

### Acknowledgements

The authors thank Jorge Mondejar-Durán for the technical advice and discussions with TBARS experiments. The study sponsors were not involved in the design of the study, the collection, analysis and interpretation of data, or writing the report, and did not impose any restrictions regarding the publication of the report.

### Competing interests

Steve Lassueur, Antonio Núñez Galindo, Loïc Dayon and Andreas Wiederkehr were employed by Société des Produits Nestlé S.A. during the generation of this manuscript.

### Author contributions

Conceptualization: J.S., A.W.; Methodology: P.A., S.R., E.C., S.D.; Investigation: S.L., A.N., S.D.; Data curation: J.S., A.N., L.D., A.W.; Writing - original draft: J.S., A.W.; Writing - review & editing: J.S., A.W.; Supervision: J.S., L.D., A.W.

### Funding

This study was funded by Nestle Research (Switzerland), Programa Estratégico Instituto de Biología y Genética Molecular (IBGM) de Valladolid. Ref. CCVC8485 (Spain) and Proyecto de Internacionalización de la Unidad de Excelencia Instituto de Biología y Genética Molecular (IBGM) de Valladolid, Ref. CL-EI-2021 IBGM (Spain).

### Data availability

All relevant data can be found within the article and its supplementary information.

### Peer review history

The peer review history is available online at <https://journals.biologists.com/jcs/lookup/doi/10.1242/jcs.260049.reviewer-comments.pdf>

### References

- Abrams, A. J., Fontanesi, F., Tan, N. B. L., Buglo, E., Campeanu, I. J., Rebelo, A. P., Kornberg, A. J., Phelan, D. G., Stark, Z. and Zuchner, S. (2018). Insights into the genotype-phenotype correlation and molecular function of SLC25A46. *Hum. Mutat.* **39**, 1995-2007. doi:10.1002/humu.23639
- Abrams, A. J., Hufnagel, R. B., Rebelo, A., Zanna, C., Patel, N., Gonzalez, M. A., Campeanu, I. J., Griffin, L. B., Groenewald, S., Strickland, A. V. et al. (2015). Mutations in SLC25A46, encoding a UGO1-like protein, cause an optic atrophy spectrum disorder. *Nat. Genet.* **47**, 926-932. doi:10.1038/ng.3354
- Antinozzi, P. A., Ishihara, H., Newgard, C. B. and Wollheim, C. B. (2002). Mitochondrial metabolism sets the maximal limit of fuel-stimulated insulin secretion in a model pancreatic beta cell: a survey of four fuel secretagogues. *J. Biol. Chem.* **277**, 11746-11755. doi:10.1074/jbc.M108462200
- de Marchi, U., Thevenet, J., Hermant, A., Dioum, E. and Wiederkehr, A. (2014). Calcium co-regulates oxidative metabolism and ATP synthase-dependent respiration in pancreatic beta cells. *J. Biol. Chem.* **289**, 9182-9194. doi:10.1074/jbc.M113.513184
- de Vos, A., Heimberg, H., Quartier, E., Huypens, P., Bouwens, L., Pipeleers, D. and Schuit, F. (1995). Human and rat beta cells differ in glucose transporter but not in glucokinase gene expression. *J. Clin. Invest.* **96**, 2489-2495. doi:10.1172/JCI118308

- Eizirik, D. L., Korbitt, G. S. and Hellerström, C. (1992). Prolonged exposure of human pancreatic islets to high glucose concentrations in vitro impairs the beta-cell function. *J. Clin. Invest.* **90**, 1263-1268. doi:10.1172/JCI115989
- El-Assaad, W., Buteau, J., Peyot, M. L., Nolan, C., Roduit, R., Hardy, S., Joly, E., Dbaibo, G., Rosenberg, L. and Prentki, M. (2003). Saturated fatty acids synergize with elevated glucose to cause pancreatic beta-cell death. *Endocrinology* **144**, 4154-4163. doi:10.1210/en.2003-0410
- Frezza, C., Cipolat, S., Martins de Brito, O., Micaroni, M., Beznoussenko, G. V., Rudka, T., Bartoli, D., Polshuck, R. S., Danial, N. N. et al. (2006). OPA1 controls apoptotic cristae remodeling independently from mitochondrial fusion. *Cell*, **126**, 177-189. doi:10.1016/j.cell.2006.06.025
- Germain, M., Mathai, J. P., McBride, H. M. and Shore, G. C. (2005). Endoplasmic reticulum BIK initiates DRP1-regulated remodeling of mitochondrial cristae during apoptosis. *EMBO J.* **24**, 1546-1556. doi:10.1038/sj.emboj.7600592
- Griesche, N., Sanchez, G., Hermans, C. and Idevall-Hagren, O. (2019). Cortical mitochondria regulate insulin secretion by local Ca<sup>2+</sup> buffering in rodent beta cells. *J. Cell Sci.* **132**, jcs228544. doi:10.1242/jcs.228544
- Heit, J. J., Apelqvist, Å. A., Gu, X., Winslow, M. M., Neilson, J. R., Crabtree, G. R. and Kim, S. K. (2006). Calcineurin/NFAT signalling regulates pancreatic beta-cell growth and function. *Nature* **443**, 345-349. doi:10.1038/nature05097
- Hellman, B., Idahl, L. A., Lernmark, A., Sehlin, J. and Täljedal, I. B. (1974). The pancreatic beta-cell recognition of insulin secretagogues. Effects of calcium and sodium on glucose metabolism and insulin release. *Biochem. J.* **138**, 33-45. doi:10.1042/bj1380033
- Hennings, T. G., Chopra, D. G., DeLeon, E. R., VanDeusen, H. R., Sesaki, H., Merrins, M. J. and Ku, G. M. (2018). In Vivo deletion of  $\beta$ -Cell Drp1 impairs insulin secretion without affecting islet oxygen consumption. *Endocrinology* **159**, 3245-3256. doi:10.1210/en.2018-00445
- Janer, A., Prudent, J., Paupe, V., Fahiminiya, S., Majewski, J., Sgarlato, N., des Rosiers, C., Forest, A., Lin, Z., Gingras, A. et al. (2016). SLC25A46 is required for mitochondrial lipid homeostasis and cristae maintenance and is responsible for Leigh syndrome. *EMBO Mol. Med.* **8**, 1019-1038. doi:10.15252/emmm.201506159
- Jansson, D., Ng, A. C. H., Fu, A., Depatie, C., al Azzabi, M. and Sreaton, R. A. (2008). Glucose controls CREB activity in islet cells via regulated phosphorylation of TORC2. *Proc. Natl. Acad. Sci. U.S.A.* **105**, 10161-10166. doi:10.1073/pnas.0800796105
- Jhun, B. S., Lee, H., Jin, Z. G. and Yoon, Y. (2013). Glucose stimulation induces dynamic change of mitochondrial morphology to promote insulin secretion in the insulinoma cell line INS-1E. *PLoS One* **8**, e60810.
- Kabra, U. D., Pfuhlmann, K., Migliorini, A., Keipert, S., Lamp, D., Korsgren, O., Gegg, M., Woods, S. C., Pfluger, P. T., Lickert, H. et al. (2017). Direct substrate delivery into mitochondrial fission-deficient pancreatic islets rescues insulin secretion. *Diabetes* **66**, 1247-1257. doi:10.2337/db16-1088
- Kozjak-Pavlovic, V. (2017). The MICOS complex of human mitochondria. *Cell Tissue Res.* **367**, 83-93. doi:10.1007/s00441-016-2433-7
- Lee, Y. J., Jeong, S. Y., Karbowski, M., Smith, C. L. and Youle, R. J. (2004). Roles of the mammalian mitochondrial fission and fusion mediators Fis1, Drp1, and Opa1 in apoptosis. *Mol. Biol. Cell* **15**, 5001-5011. doi:10.1091/mbc.e04-04-0294
- Liesa, M., Palacín, M. and Zorzano, A. (2009). Mitochondrial dynamics in mammalian health and disease. *Physiol. Rev.* **89**, 799-845. doi:10.1152/physrev.00030.2008
- Maedler, K., Spinass, G. A., Dyntar, D., Moritz, W., Kaiser, N. and Donath, M. Y. (2001). Distinct effects of saturated and monounsaturated fatty acids on beta-cell turnover and function. *Diabetes* **50**, 69-76. doi:10.2337/diabetes.50.1.69
- Mitra, K. and Lippincott-Schwartz, J. (2010). Analysis of mitochondrial dynamics and functions using imaging approaches. *Curr. Protoc. Cell Biol.* Chapter 4: Unit 4.25.1-21. doi:10.1002/0471143030.cb0425s46
- Molina, A. J. A., Wikstrom, J. D., Stiles, L., Las, G., Mohamed, H., Elorza, A., Walzer, G., Twig, G., Katz, S., Corkey, B. E. et al. (2009). Mitochondrial networking protects beta-cells from nutrient-induced apoptosis. *Diabetes* **58**, 2303-2315. doi:10.2337/db07-1781
- Nakano, K., Yanobu-Takanashi, R., Shimizu, Y., Takahashi, Y., Hiura, K., Watanabe, M., Sasaki, H., Okamura, T. and Sasaki, N. (2020). Genetic locus responsible for diabetic phenotype in the insulin hyposecretion (ihs) mouse. *PLoS One* **15**, e0234132.
- Neupert, W. (2012). SnapShot: Mitochondrial architecture. *Cell* **149**, 722-722.e1. doi:10.1016/j.cell.2012.04.010
- Olichon, A., Baricault, L., Gas, N., Guillou, E., Valette, A., Belenguer, P. and Lenaers, G. (2003). Loss of OPA1 perturbs the mitochondrial inner membrane structure and integrity, leading to cytochrome c release and apoptosis. *J. Biol. Chem.* **278**, 7743-7746. doi:10.1074/jbc.C200677200
- Palmieri, F. (2013). The mitochondrial transporter family SLC25: identification, properties and physiopathology. *Mol. Asp. Med.* **34**, 465-484. doi:10.1016/j.mam.2012.05.005
- Park, K. S., Wiederkehr, A., Kirkpatrick, C., Mattenberger, Y., Martinou, J. C., Marchetti, P., Demareux, N. and Wollheim, C. B. (2008). Selective actions of mitochondrial fission/fusion genes on metabolism-secretion coupling in insulin-releasing cells. *J. Biol. Chem.* **283**, 33347-33356. doi:10.1074/jbc.M806251200
- Pich, S., Bach, D., Briones, P., Liesa, M., Camps, M., Testar, X., Palacín, M. and Zorzano, A. (2005). The Charcot-Marie-Tooth type 2A gene product, Mfn2, up-regulates fuel oxidation through expression of OXPHOS system. *Hum. Mol. Genet.* **14**, 1405-1415. doi:10.1093/hmg/ddi149
- Reinhardt, F., Schultz, J., Waterstradt, R. and Baltrusch, S. (2016). Drp1 guarding of the mitochondrial network is important for glucose-stimulated insulin secretion in pancreatic beta cells. *Biochem. Biophys. Res. Commun.* **474**, 646-651. doi:10.1016/j.bbrc.2016.04.142
- Rorsman, P. and Ashcroft, F. M. (2018). Pancreatic  $\beta$ -cell electrical activity and insulin secretion: of mice and men. *Physiol. Rev.* **98**, 117-214. doi:10.1152/physrev.00008.2017
- Ruprecht, J. J. and Kunji, E. R. S. (2020). The SLC25 mitochondrial carrier family: structure and mechanism. *Trends Biochem. Sci.* **45**, 244-258. doi:10.1016/j.tibs.2019.11.001
- Santo-Domingo, J., Galindo, A. N., Cominetti, O., de Marchi, U., Cutillas, P., Dayon, L. and Wiederkehr, A. (2019). Glucose-dependent phosphorylation signaling pathways and crosstalk to mitochondrial respiration in insulin secreting cells. *Cell Commun. Signal.* **17**, 14. doi:10.1186/s12964-019-0326-6
- Schuit, F., de Vos, A., Farfari, S., Moens, K., Pipeleers, D., Brun, T. and Prentki, M. (1997). Metabolic fate of glucose in purified islet cells. Glucose-regulated anaplerosis in beta cells. *J. Biol. Chem.* **272**, 18572-18579. doi:10.1074/jbc.272.30.18572
- Sreaton, R. A., Conkright, M. D., Katoh, Y., Best, J. L., Canettieri, G., Jeffries, S., Guzman, E., Niessen, S., Yates, J. R., Takemori, H. et al. (2004). The CREB coactivator TORC2 functions as a calcium- and cAMP-sensitive coincidence detector. *Cell* **119**, 61-74. doi:10.1016/j.cell.2004.09.015
- Sesaki, H. and Jensen, R. E. (2001). UGO1 encodes an outer membrane protein required for mitochondrial fusion. *J. Cell Biol.* **152**, 1123-1134. doi:10.1083/jcb.152.6.1123
- Sesaki, H. and Jensen, R. E. (2004). Ugo1p links the Fzo1p and Mgm1p GTPases for mitochondrial fusion. *J. Biol. Chem.* **279**, 28298-28303. doi:10.1074/jbc.M401363200
- Shah, P., Ardestani, A., Dharmadhikari, G., Laue, S., Schumann, D. M., Kerr-Conte, J., Pattou, F., Klein, T. and Maedler, K. (2013). The DPP-4 inhibitor linagliptin restores  $\beta$ -cell function and survival in human isolated islets through GLP-1 stabilization. *J. Clin. Endocrinol. Metab.* **98**, 7. doi:10.1210/jc.2013-1029
- Steffen, J., Vashisht, A. A., Wan, J., Jen, J. C., Claypool, S. M., Wohlschlegel, J. A. and Koehler, C. M. (2017). Rapid degradation of mutant SLC25A46 by the ubiquitin-proteasome system results in MFN1/2-mediated hyperfusion of mitochondria. *Mol. Biol. Cell* **28**, 600-612. doi:10.1091/mbc.e16-07-0545
- Twig, G., Elorza, A., Molina, A. J. A., Mohamed, H., Wikstrom, J. D., Walzer, G., Stiles, L., Haigh, S. E., Katz, S., Las, G. et al. (2008). Fission and selective fusion govern mitochondrial segregation and elimination by autophagy. *EMBO J.* **27**, 433-446. doi:10.1038/sj.emboj.7601963
- Wan, J., Steffen, J., Yourshaw, M., Mamsa, H., Andersen, E., Rudnik-Schöneborn, S., Pope, K., Howell, K. B., Mclean, C. A., Kornberg, A. J. et al. (2016). Loss of function of SLC25A46 causes lethal congenital pontocerebellar hypoplasia. *Brain: A Journal of Neurology* **139**, 2877-2890. doi:10.1093/brain/aww212
- Wiederkehr, A. and Wollheim, C. B. (2012). Mitochondrial signals drive insulin secretion in the pancreatic  $\beta$ -cell. *Mol. Cell. Endocrinol.* **353**, 128-137. doi:10.1016/j.mce.2011.07.016
- Zhang, Z., Wakabayashi, N., Wakabayashi, J., Tamura, Y., Song, W. J., Sereda, S., Clerc, P., Polster, B. M., Aja, S. M., Pletnikov, M. V. et al. (2011). The dynamin-related GTPase Opa1 is required for glucose-stimulated ATP production in pancreatic beta cells. *Mol. Biol. Cell* **22**, 2235-2245. doi:10.1091/mbc.e10-12-0933